Nanotopographical surfaces for regulating cellular mechanical behaviors investigated by atomic force microscopy

Mi Li[1, 2*], Ning Xi[3], Yuechao Wang[1, 2], Lianqing Liu[1, 2*]

[1]State Key Laboratory of Robotics, Shenyang Institute of Automation, Chinese Academy of Sciences, Shenyang 110016, China

[2]Institutes for Robotics and Intelligent Manufacturing, Chinese Academy of Sciences, Shenyang 110016, China

[3]Department of Industrial and Manufacturing Systems Engineering, The University of Hong Kong, Hong Kong, China

*Corresponding authors (e-mail: limi@sia.cn; lqliu@sia.cn)

Abstract Cell-substrate interactions play an important role in regulating cellular physiological and pathological processes and therefore investigating cell-substrate interface is meaningful for understanding the behaviors of cells. However, so far the underlying mechanisms which guide the nanoscopic biological activities taking place at the cell-substrate interface remain poorly understood. The advent of atomic force microscopy (AFM) provides a powerful tool for characterizing the structures and properties of native biological and biomaterial systems with unprecedented spatiotemporal resolution, which offers new possibilities for understanding the physical sciences of biomaterials. Here, AFM was utilized to unravel the nanotopographical surfaces for regulating cellular behaviors on three different substrates (glass slide, mica, and petri dish). Firstly, the decellularized substrates prepared with the use of ammonia and trypsin were imaged by AFM, significantly showing the nanogranular substances on the decellularized substrates as well as the cell membrane patches for uncovering the detailed situations of mechanical contact between cells and substrates. Next, experiments performed on chemically fixed substrates with the use of paraformaldehyde together with AFM time-lapse imaging remarkably showed that nanogranular depositions from cell culture medium appeared on the substrates for promoting cell growth. Further, the detailed cell culture medium components which contribute to the nanogranular depositions are identified. Finally, the dynamic alterations in surface roughness and mechanical properties of substrates and cells during cell growth were quantitatively measured by AFM force spectroscopy, revealing the diverse changes of the multiple physical properties (surface roughness, adhesion force, Young's modulus, and relaxation time) during cell-substrate interactions. The research provides novel insights into the nanotopographical surfaces for cell-substrate interactions, which will be useful for understanding cellular behaviors.

Keywords atomic force microscopy, cell-substrate interactions, nanotopographical surface, nanogranular deposition, surface roughness, mechanical properties

1. Introduction

Cell-substrate interactions play an important role in guiding the physiological and pathological processes of cells. Cells reside in a microenvironment which is composed of extracellular matrix (ECM), soluble factors, and other cells (e.g., vascular endothelial, stromal and immune cells [1]). Though biochemical communities have long known the regulatory roles of soluble signals (e.g., growth factor, cytokine) in cell fate determination, evidence in the past years has strongly witnessed that the insoluble ECM participates in directing cellular behaviors [2]. ECM not only provides physical support for cellular adherence and growth, but also initiates biochemical and biomechanical cues that are required for tissue morphogenesis, differentiation and homeostasis [3]. Cells bind to the ECM *via* the integrin molecules (a type of transmembrane receptor) which distribute on the surface of cells [4], allowing the cells to sense the mechanical stimuli exerted by ECM [5]. The external mechanical clues are then transmitted to cellular nucleus by a series of subcellular structures (e.g., cytoskeleton, cytoplasm, proteins) through the mechanism of mechanotransduction [6], which eventually influences the gene expression [7] and biological behaviors of cells

(e.g., cell motility, cell spreading) [8]. ECM may become abnormal (e.g., the amount, composition, or topography of the ECM turn aberrant), which will affect the functions of ECM and subsequently promote the appearance of diseases such as cancer [9]. Generally tumor tissues are significantly stiffer than the healthy tissues, which is mainly due to the increased ECM deposition in cancers [10]. The ECM remodeling (e.g., collagen fiber alignment, bundling, and stiffening) in turn alters the interactions between ECM and cells to enhance pro-angiogenic secretion from a range of cells in the microenvironment [11], which contributes to the migration and metastasis of cancerous cells [12]. Consequently, investigating cell-substrate interactions is useful for fundamentally understanding the underlying mechanisms guiding cellular behaviors.

Designing substrates with defined structures and properties to mimic the ECM of cells have emerged as a promising way to direct the behaviors of cells for biomedical applications. ECM varies in the composition and concentration for different tissues, and also different types of cells interact with ECM in various ways [13]. A number of two-dimensional (2D) (e.g., flat substrate) and three-dimensional (3D) (e.g., hydrogel) biomaterials have been utilized to act as substrates for controlling cell fates *in vitro*, which have achieved notable applications in diverse fields, including stem cell and cancer research, cell therapy, tissue engineering, immunomodulation, and diagnostics [14, 15]. The 2D approaches allow well-controlled analysis of the impact of individual components of the microenvironment on cells, while the 3D approaches allow reconstruction and realization of the complexity of the microenvironment [16]. With the use of substrates possessing different physical properties (e.g., patterned topography, surface geometry and mechanics) [17, 18], integrated with adhesion ligands, such as peptides (RGD) and proteins (e.g., collagen, fibronectin, laminin) [19, 20], the behaviors of stem cells can be tuned for regenerative medicine. The biomaterials mimicking ECM are also able to serve as building blocks for engineering tumor microenvironment, which recapitulate various microenvironmental cues of human tumors, benefiting drug screening of anticancer therapeutics [21]. In addition, dynamically tunable cell culture platforms where the biochemical and mechanostructural properties of ECM are modulated over time in a user-defined manner have been developed based on natural polymers or synthetic polymers, allowing better understanding the intricate cellular microenvironments and promoting the studies of cell mechanobiology [22].

Despite the fundamental role of cell-substrate interactions in designing ECM analogue to regulate cellular behaviors for biomedical applications, so far information about the detailed cell-substrate interface at the nanoscale is still limited. In this work, atomic force microscopy (AFM), a powerful label-free tool for characterizing native biological and biomaterial systems with nanometer spatial resolution [23, 24], was utilized to uncover the nanoscopic cell-substrate interactions taking place on three different substrates (glass slide, mica, Petri dish) with the use of three different types of cells (C2C12, HEK293, MCF-7). The nanotopographical surfaces of decellularized and native substrates were visualized with the use of three biochemical reagents, including ammonia, trypsin, and paraformaldehyde (PFA), considerably showing that the nanogranular biological depositions from cell culture medium contribute to the cell growth. The dynamic changes in the surface roughness and mechanical properties (adhesion force, Young's modulus, and relaxation time) of substrates and cells during cell growth were investigated. The experimental results provide novel insights into nanoscopic cell-substrate interface, which will benefit the studies about cellular behaviors.

2. Materials and Methods

2.1 Cell culture and reagents

C2C12 (mouse myoblast cell line), HEK293 (human embryonic kidney cell line), and MCF-7 (human breast cancer cell line) cells were purchased from the Cell Bank of Chinese Academy of Sciences (Shanghai, China). Cells were cultured in DMEM medium with high glucose (Hyclone Laboratories, Logan, UT, USA) containing 10% fetal bovine serum (Biological Industries, Kibbutz Beit-Haemek, Israel) and 1% penicillin-streptomycin solution (Hyclone Laboratories, Logan, UT, USA) at

37℃(5% CO_2 and 95% air). Ammonia (NH_4OH) was purchased from Sigma-Aldrich Company (St. Louis, MO, USA). Phosphate buffered saline (PBS) was purchased from Hyclone Laboratories (Logan, UT, USA). Trypsin solution (0.25%) containing ethylenediaminetetraacetic acid (EDTA) was purchased from Thermo Fisher Scientific Company (Waltham, Massachusetts, USA). Paraformaldehyde (PFA) (4%) and acridine orange (AO) dye were purchased from Solarbio Life Sciences Company (Beijing, China). The Milli-Q pure water (Merck KGaA Company, Darmstadt, Germany) was used in the experiments. Cells were cultured in Petri dishes. Once cells reached 80% confluence, cells were passaged with the use of trypsin-EDTA and then incubated for 2-3 days before experiments.

Three types of substrates, including glass slides, mica, and Petri dish (the material is polystyrene and dish is surface treated), were used to grow cells. For growing cells on glass slides, fresh glass slides were placed in a Petri dish which was then moved into the biosafety cabinet (Thermo Fisher Scientific, Waltham, Massachusetts, USA) for ultraviolet sterilization (1 h). Then cells were seeded in the Petri dish containing glass slides and incubated at 37℃(5% CO_2 and 95% air). For culturing cells on mica, a piece of mica was attached onto a glass slide *via* a double faced adhesive. After removing the top layer of the mica, the glass slide containing mica was placed in a Petri dish which was then moved into the biosafety cabinet for ultraviolet sterilization and subsequently cells were seeded in the Petri dish containing mica. For growing cells on Petri dish, cells were directly seeded in the regular Petri dish which did not containing glass slides or mica after ultraviolet sterilization. Once cells grown on substrates reached 50% confluence, the cell samples were used for experiments.

2.2 Sample preparation

Ammonia (NH_4OH) was used to obtain the decellularized glass slides. Firstly, the original NH_4OH solution (1 M) was diluted to final concentrations (0.02 M or 0.04 M) with the use of pure water. Then the cell culture medium of the Petri dish containing glass slides (cells were grown on the glass slides) was removed. Next, the diluted NH_4OH solution was added into the Petri dish and incubated at room temperature for a period of time (5 min, 15 min, or 30 min). After incubation, the NH_4OH solution in the Petri dish was removed and the glass slides in the Petri dish were washed by pure water for three times. Subsequently, the glass slides were left in air for natural drying, after which the glass slides were placed onto the sample stage of AFM for AFM observations.

The decellularized glass slides were also obtained with the use of trypsin-EDTA. Firstly, the cell culture medium of the Petri dish containing glass slides on which cells were grown was removed. Then 2 mL trypsin-EDTA solution was added into the Petri dish and incubated at room temperature for a period of time (1 min, 2 min). After incubation, the trypsin-EDTA solution in the Petri dish was removed. Next, pure water was added into the Petri dish and then the micropipette was used to perform aspiration and discharging on the glass slides to remove cells from the glass slides. Then the glass slides were washed by pure water and left in air for drying, after which AFM scanning on the decellularized glass slides was performed.

The native substrates were obtained with the use of PFA. Firstly, the cell culture medium of the Petri dish (either containing glass slides/mica or not) in which cells were grown was removed. Then 4% PFA solution was added into the Petri dish and incubated for 30 min at room temperature. After incubation, the substrates were washed by pure water for three times. Subsequently, the substrates were scanned by AFM after air drying.

2.3 Optical and fluorescent microscopy

Optical and fluorescent images of cells grown on the substrates were obtained with the use of an inverted fluorescence microscope (Ti, Nikon, Tokyo, Japan). The glass slides (after being treated by ultraviolet sterilization) were previously placed in a petri dish containing cell culture medium and then incubated at 37℃(5% CO2 and 95% air) for 24 h. After incubation,

cells (C2C12, HEK293, or MCF-7) were seeded on the glass slides in dishes and then cultured at 37℃(5% CO2 and 95% air) for 24 h. For control, bare glass slides without being treated by cell culture medium in advance were also used to grow cells for 24 h. Subsequently, AO dye solution was added into the dishes (the final concentration was 20 μg/mL) and then the dishes were incubated at 37℃(5% CO2 and 95% air) for 15 min. After the incubation, the dishes were placed onto the sample stage of the inverted fluorescence microscope and then optical and fluorescent images of cells were recorded.

2.4 Atomic force microscopy

AFM experiments were performed with the use of a commercial AFM called Dimension Icon AFM (Bruker, Santa Barbara, CA, USA). AFM images of substrates were obtained at peak force tapping imaging mode. The nominal spring constant of the cantilever used for AFM imaging was 0.4 N/m and the nominal spring constant of the cantilever used for mechanical measurements was 0.01 N/m. The accurate spring constant of the cantilever was calibrated during AFM experiments. Under the guidance of the AFM's optical microscopy, the probe was moved to the substrates. Force curves were obtained on the stiff substrates to calibrate the deflection sensitivity of the cantilever, which was then used to exactly calibrate the spring constant of the cantilever by the thermal noise module of AFM. The scan line was 512 and the sampling points for each scan line was also 512. The scanning rate was 1 Hz.

AFM cellular mechanical properties (cellular adhesion force, cellular Young's modulus, cellular relaxation time) were measured by controlling AFM tip to vertically perform approach-dwell-retract cycle [25] on the living cells grown on different substrates in cell culture medium. Under the guidance of optical microscopy, AFM tip was moved to the cells. Subsequently, AFM tip was controlled to perform approach-dwell-retract movements on the central areas of the cells at the AFM force ramp mode. Firstly, the AFM probe above the cell gradually approached and indented the cells, which caused the deflections of the AFM cantilever. When the force exerted on the cantilever achieved the preset value (1 nN), the probe stopped approaching and then dwelt on the cells for a period of time (1 s). After the stage of dwelling, the AFM tip retracted from the cells and returned to its original position. During the approach-dwell-retract process, the vertical displacements of probe and the deflections of cantilever were recorded by the AFM manipulation software Nanoscope Analysis (Bruker, Santa Barbara, CA, USA), which yielded the force-distance (F-D) curves. F-D curves were used to calculate cellular Young's modulus. At the same time, the changes of amplitude signals of AFM cantilever were recorded by an oscilloscope (LeCroy, New York, USA) linked to AFM, which yielded the force-time (F-T) curves. F-T curves were used to calculate cellular relaxation time. The ramp rate was 1 Hz and the ramp size was 6 μm during the approach-dwell-retract cycle. For each types of cells (C2C12, HEK293, MCF-7) and each types of substrates (glass slides, mica, Petri dish), F-D curves and F-T curves were obtained on twenty cells to obtain statistical data. Since the cellular Young's modulus and cellular relaxation time probed by AFM are dependent on the measurement parameters, such as surface dwell time and tip approaching rate [26, 27], the measurement parameters were kept identical during the experiments to make the results comparable.

2.5 Data analysis

The surface roughness was calculated from the AFM height images [28]:

$$R_q = \sqrt{\frac{\sum Z_i^2}{N}} \tag{1}$$

where R_q is the root-mean-square roughness taken from the AFM height images, N is the number of pixel points within the selected regions of AFM height images, and Z_i is the height values of the i^{th} pixel points. The calculation of Rq was performed with the use of AFM offline software Nanoscope Analysis (Bruker, Santa Barbara, CA, USA). From the AFM images of substrates obtained at large scan sizes (such as 4×4 μm^2), region areas with smaller sizes (e.g., 200×200 nm^2, 400×400 nm^2,

600×600 nm^2, 800×800 nm^2, 1×1 μm^2) could be selected and the roughness values of these selected region areas could then be calculated (as shown in Fig. S1) to analyze the surface roughness at different scales.

The adhesion force was calculated by analyzing the retract curves of the recorded F-D curves. Baseline correction was firstly performed on the recorded original F-D curves with the use of AFM manipulation software Nanoscope Analysis (Bruker, Santa Barbara, CA, USA). Then the retract portions of F-D curves were exported as test files. Subsequently, the test files were imported to Matlab (MathWorks, Natick, Massachusetts, USA). With the use of Matlab, the adhesion force (corresponding to the peak forces below the baseline) of the retract curve was calculated.

The cellular Young's modulus was obtained by fitting the approach portion of the recorded F-D curves with Hertz-Sneddon model [29]:

$$F_{\text{spherical}} = \frac{4E\delta^{1.5}\sqrt{R}}{3(1-\upsilon^2)} \tag{2}$$

$$F_{\text{conical}} = \frac{2E\delta^2\tan\theta}{\pi(1-\upsilon^2)} \tag{3}$$

where υ is the Poisson ratio of cell (cells are often considered as incompressible materials and thus υ=0.5), F is the loading force exerted by AFM probe, δ is the indentation depth, E is the Young's modulus of cell, θ is the half-opening angle of conical tip, and R is the radius of spherical tip. The loading force F could be obtained from the cantilever deflection by Hooke's law:

$$F = kx \tag{4}$$

where k is the spring constant of the cantilever, and x is the deflection of cantilever. The cantilever deflection x is detected by a four-quadrant photodiode detector which is capable of sensing a beam of laser reflected off the backside of the cantilever. According to the contact point visually determined in the approach curve, the approach curve is converted into the indentation curve by subtracting the cantilever deflection from the vertical movement of the probe [25]. The indentation curve is then fitted by Hertz-Sneddon model to obtain cellular Young's modulus. Hertz model is applicable for spherical tip, while Sneddon extended Hertz model to conical tip [29]. Since conical tip was used here, Sneddon model was used for calculation of cellular Young's modulus. Notably, Hertz-Sneddon model is based on several assumptions, such as homogeneous, isotropic, and infinitely thick. Nevertheless, studies have shown that Hertz-Sneddon model is applicable when the indentation into the cell is much smaller than the thickness of cell [30]. In practice, Hertz-Sneddon model is the most widely used model for calculating cellular Young's modulus [31, 32] from the F-D curves obtained during AFM force spectroscopy. Fitting the indentation curves with Sneddon model was performed with the program written by Matlab.

The cellular relaxation time was obtained by fitting the F-T curves with two-order Maxwell model [29]:

$$F(t) = A_0 + A_i \sum_{i=1}^{2} e^{-t/\tau_i} \tag{5}$$

$$\tau_i = \frac{\eta_i}{E_i} \tag{6}$$

where F is the applied loading force, A_0 is the instantaneous (purely elastic) response, A_i are the i$^{\text{th}}$ force amplitudes, τ_i is the i$^{\text{th}}$ cellular relaxation time, η_i is the i$^{\text{th}}$ cellular viscosity, and E_i is the i$^{\text{th}}$ cellular Young's modulus. The cellular relaxation time (τ) is the ratio of cellular viscosity (η) to cellular Young's modulus (E), and thus cellular relaxation time reflects the viscoelastic properties of cells. The recorded original F-T curves were imported to Matlab (MathWorks, Natick, Massachusetts, USA). Then the relaxation portion of F-T curves was normalized. Subsequently, two-order Maxwell model was used to fit the normalized relaxation curves, which yielded two relaxation times (τ_1 and τ_2). The Maxwell fitting was performed with the use of the commercial software Abaqus (Dassault Systems Simulia Corp., RI, USA). The illustrational process of extracting the cellular relaxation time from the relaxation curves is shown in Fig. S2.

3. Results and Discussion

3.1 Decellularized substrates are coated by nanogranular biological depositions

Fig. 1 shows the schematic of utilizing AFM to investigate the details of nanotopographical cues involved in cell-substrate interactions. On the one hand, nanogranular biological depositions coated on the substrates during cell culture were clearly observed and analyzed (Fig. 1A). On the other hand, topographical and mechanical changes of substrates and cells during cell growth were revealed. Three types of substrates (glass slide, mica, Petri dish) which have different surface topographical features were used in this study. Glass slide has a flat and rough surface (Fig. 1B). The surface of freshly cleaved mica is flat and smooth (Fig. 1C). Petri dish (made of polystyrene) which is widely used in cell culture has patterned surface (Fig. 1D) containing scaffold structures (I in Fig. 1D) particle-like structures (II in Fig. 1D).

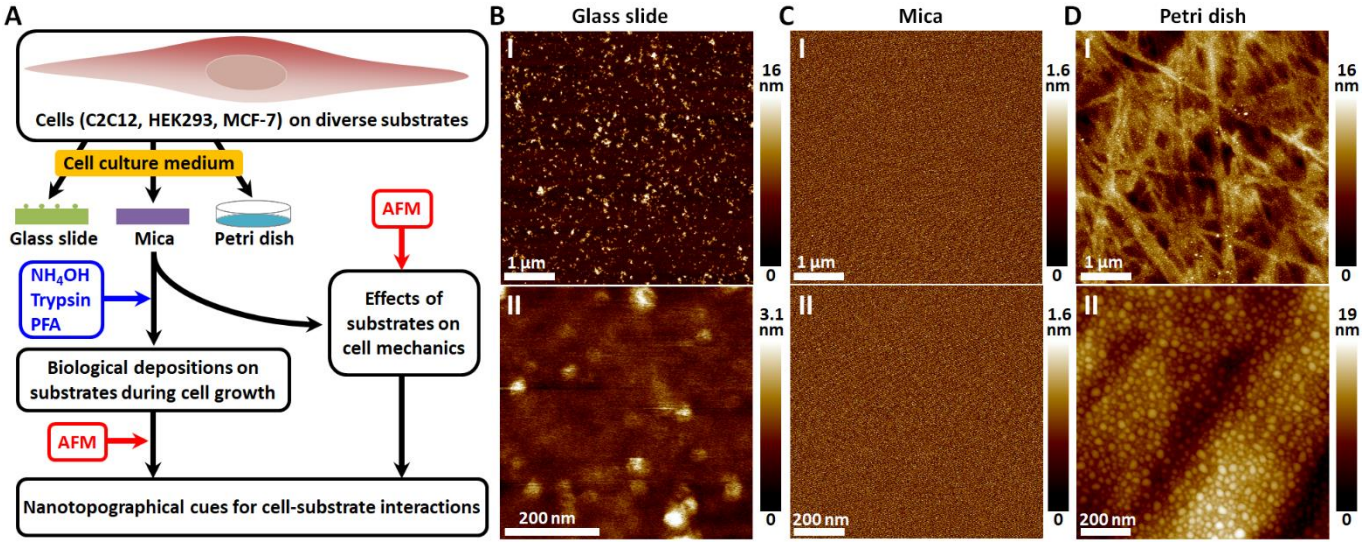

Figure 1 Investigating nanoscopic cell-substrate interactions on three types of substrates (glass slide, mica, Petri dish) by AFM. (A) Schematic of observing cell-substrate interactions at the nanoscale. After culturing cells (C2C12 cells, HEK293 cells, or MCF-7 cells) on the substrates (glass slide, mica, or Petri dish), the biological depositions coated on the substrates during cell culture are obtained with the use of different biochemical reagents, including ammonia (NH_4OH), trypsin, and paraformaldehyde (PFA). AFM imaging and mechanical measurements are performed on biological depositions and cells respectively to reveal the nanotopographical cues involved in cell-substrate interactions. (B, C, D) AFM height images of the three different substrates used in the study. (B) Glass slide. (C) Mica. (C) Petri dish. AFM images were recorded in air. (I) Large-size scan images. (II) Small-size scan images.

Nanogranular depositions on the decellularized substrates prepared by ammonia or trypsin were visualized and analyzed by AFM topographical imaging. Ammonia and trypsin have been widely used to prepare decellularized matrix for tissue engineering [33-36], but so far the detailed structures of the decellularized matrix at the nanoscale remain poorly understood. Here AFM was utilized to visualize the fine structures of decellularized substrates. For each of the three different types of cell lines, AFM topographical images strikingly show that nanogranular substances widely distribute on the decellularized substrates prepared by ammonia (Fig. 2A-C). For control experiments, AFM images of bare and ammonia-treated glass slides (glass slides were placed in cell culture medium for 24 h without growing cells) also show that the substrates are covered by nanogranular substances (Fig. 2D), indicating that nanogranular substances are commonly deposited on the substrates for cell growth *in vitro*. Roughness analysis of the decellularized substrates show that on the whole that both the concentration and treatment time of ammonia influences the surface roughness of the decellularized substrates (Fig. 2E-G). Besides, we can see that there are no significant differences among the surface roughness values obtained at different sizes (200×200 nm^2, 400×400

nm^2, 600×600 nm^2, 800×800 nm^2, 1×1 μm^2), indicating the homogeneous surface roughness of the decellularized substrates. For the decellularized substrates prepared by trypsin, AFM images show the nanogranular topography of the decellularized substrates for each types of the cells used here (Fig. 3A-C). AFM images of the substrates from control groups also show the nanogranular depositions on the substrates (Fig. 3D), which is consistent with the results obtained from the control experiments by ammonia (Fig. 2D), confirming that the substrates in the cell culture medium have a layer of nanogranular substances for cell growth. Roughness analysis shows that the increase of trypsin treatment time results in the significant decrease of surface roughness of the decellularized substrates (Fig. 3E-G). The AFM images of Fig. 2 and Fig. 3 were obtained in air. We also used AFM to image the decellularized glass slides in pure water and the results (Fig. S3) show the nanogranular topography of the substrates, indicating that the nanogranular substances on the decellularized glass slides are insoluble in water and could be visualized by AFM in aqueous conditions. A notable point is whether the topographical features of glass slide itself influence the roughness of decellularized substrates. We have statistically calculated the roughness of bare glass slides (as shown in Fig. S4) and the results clearly show that bare glass slides are much smoother than the decellularized substrates observed in Fig. 2 and Fig. 3, indicating the weak influence of bare substrate surface on the decellularized substrates. Besides, the experiments in Fig. 2 and Fig. 3 are focused on examining the decellularized substrates prepared by ammonia and trypsin, and thus experiments were only performed on glass slides.

AFM high-resolution native imaging benefits understanding the fine structures of substrates for cell growth. In living organisms, cells attach to and spread on the extracellular matrix (ECM), and thus ECM and ECM-mimicking scaffolds are ideal biomaterials for tissue engineering [37]. Native ECM accurately presents a wide number of signals and components that are fundamental for the physiological activities of cells [38], and thus decellularized ECM has been used as a promising scaffold to regulate the behaviors of cells for regenerative medicine [39, 40]. Decellularized matrix has been commonly characterized by scanning electron microscopy (SEM) [41-44], which requires chemical fixation and drying of the specimen. Hence, strictly speaking, SEM cannot reflect the real topography of the specimen. Besides, SEM imaging requires gold coating of the specimen. The thickness of gold coating is usually in the ranges of 3.5-5 nm [41-44]. The size of nanogranular structures on the decellularized substrates observed here is in the range of 1.5-7 nm (as shown in Fig. S5). Therefore, the gold coating of SEM imaging may probably blur the fine structures of the specimen. Here, AFM imaging of the native decellularized substrates without pretreatments significantly reveals the previously unrecognized nanogranular structures on the decellularized substrates, indicating the nanogranular topography of the decellularized matrix and demonstrating the capabilities of AFM topographical imaging in resolving the fine structures of the decellularized matrix with unprecedented spatial resolution, which will have potential impacts on investigating cell-matrix interactions.

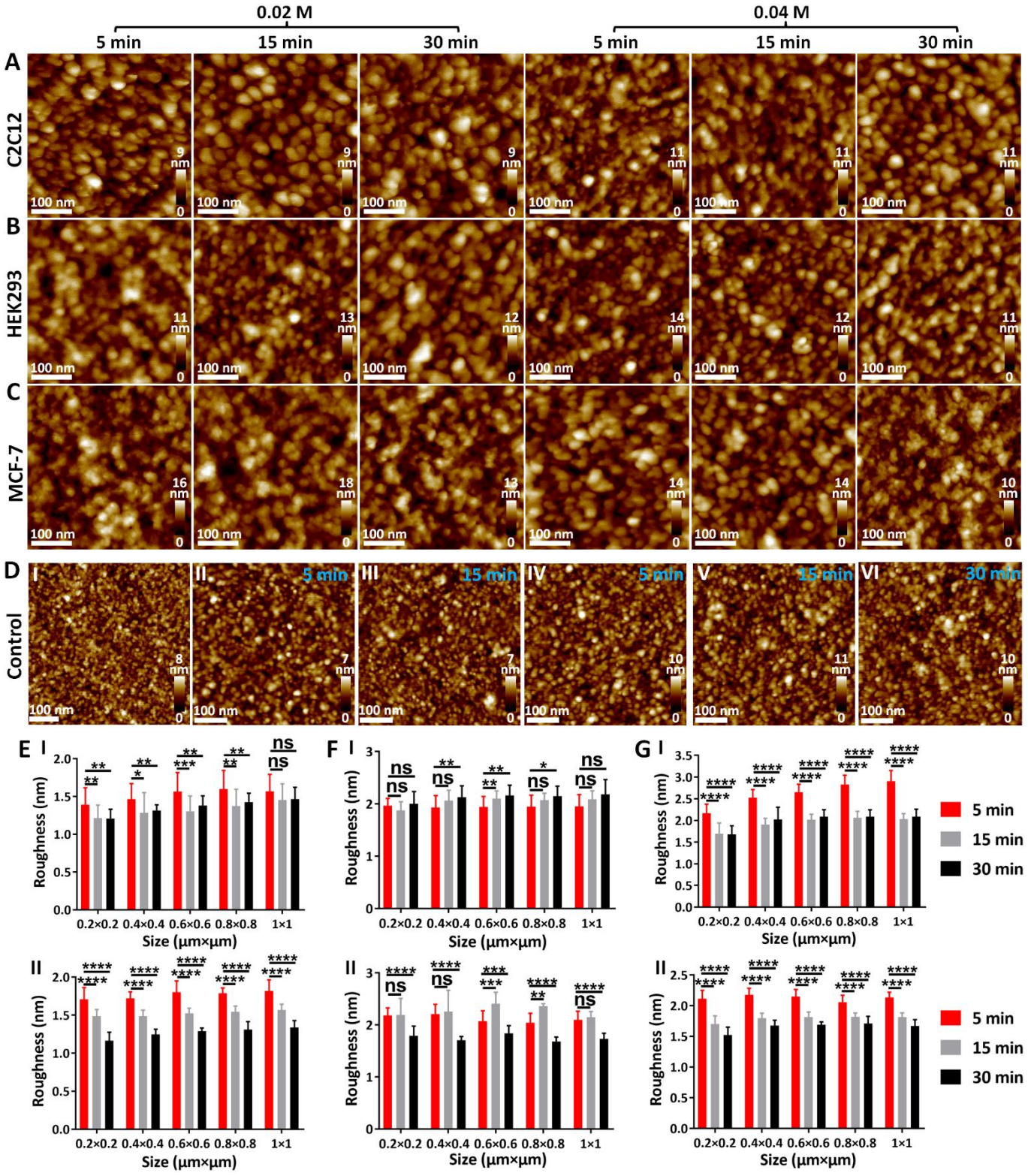

Figure 2 AFM imaging and roughness analysis of decellularized substrates prepared with the use of ammonia. The decellularized substrates were obtained by treating the glass slides (cells were grown on the glass slides) with different ammonia concentrations (0.02 M or 0.04 M) and different treatment times (5 min, 15 min, or 30 min). AFM images were recorded in air. (A, B, C) AFM height images of the decellularized substrates prepared from the glass slides growing C2C12 cells (A), HEK293 cells (B), or MCF-7 cells (C). (D) Control experiments of glass slides without growing cells. (I) Bare glass slides placed in cell culture medium for 24 h without cells. (II-VI) After being placed in cell culture medium for 24 h, bare glass slides were treated by ammonia for different times. (II, III) Treated by 0.02 M ammonia for 5 min (II) or 15 min (III). (IV-VI) Treated by 0.04 M ammonia for 5 min (IV), 15 min (V), or 30 min (VI). (E, F, G) Surface roughness (Mean±SD) of the decellularized substrates prepared from the glass slides growing C2C12 cells (E), HEK293 cells (F), or MCF-7 cells (G). (I) Ammonia concentration 0.02 M. (II) Ammonia concentration 0.04 M. N=50, *P<0.05; **p<0.01; ***p<0.001; ****p<0.0001.

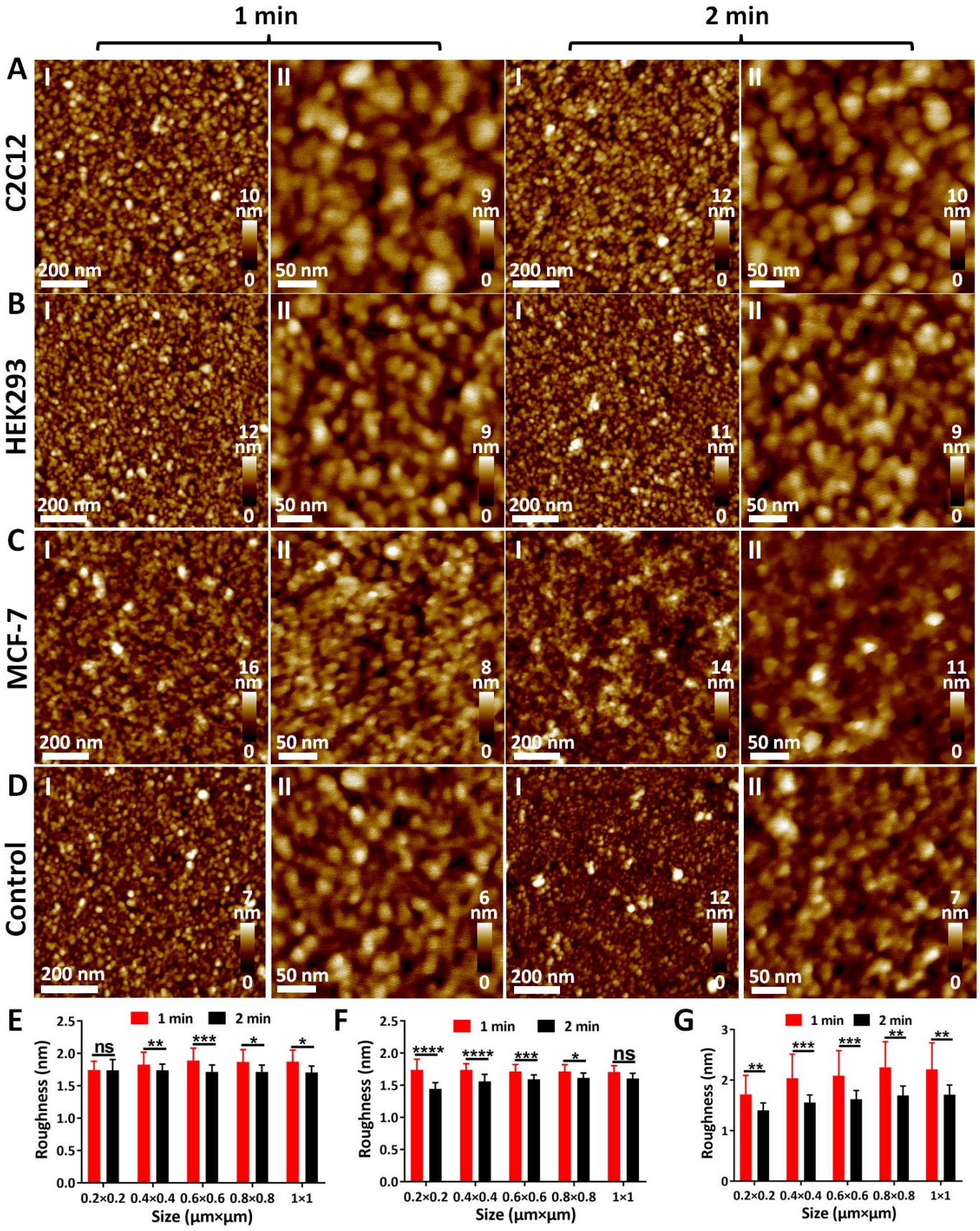

Figure 3 AFM imaging and roughness analysis of decellularized substrates prepared with the use of trypsin. The decellularized substrates were obtained by treating the glass slides (cells were grown on the glass slides) with trypsin for different treatment times (1 min, or 2 min). AFM images were recorded in air. (A, B, C) Decellularized substrates prepared from the glass slides growing C2C12 cells (A), HEK293 cells (B), or MCF-7 cells (C). (D) Control experiments of bare glass slides which were incubated in cell culture medium for 24 h without growing cells. After the incubation, the bare glass slides were treated by trypsin. (I) Large-size scan images and (II) small-size scan images. (E, F, G) Roughness (Mean±SD) analysis of the decellularized substrates growing (E) C2C12 cells, (F) HEK293 cells, or (G) MCF-7 cells. N=50, *P<0.05; **p<0.01; ***p<0.001; ****p<0.0001.

3.2 Nanogranular depositions from cell culture medium contribute to cell-substrate interactions

AFM imaging was utilized to reveal the detailed cell-substrate interface. For the decellularized glass slides (cells were grown on glass slides) prepared with trypsin, cell membrane patches were occasionally observed by AFM imaging, as shown in Fig. 4A-C. The cell membrane patches left on the decellularized substrates allow us to visualize the fine structures of cell membrane. Nanogranular structures are discernible for the cell membrane patches (II in Fig. 4A-C). The section profile curves taken along the membrane patches (III in Fig. 4A-C) indicate that the height of the membrane patches was in the range of 6-8 nm, which was consistent with the thickness of cell membrane (cell membrane usually has a thickness in the range of 5-10 nm [45]). Extra AFM images of cell membrane patches are shown in Fig. S6, confirming the nanogranular topography of cell membranes. Roughness analysis of cell membrane patches shows that the surface of MCF-7 cells is significantly rougher than that of the other two types of cells (Fig. 4D). Studies have shown that there are significant differences in cell membrane composition and organization between cancerous cells and healthy cells. For example, the glycocalyx molecules on the cell surface of cancerous cells are much larger than that on normal cells [46]. The cell surface brush layers (mainly containing microvilli, microridges and cilia) on cancerous cells are also different from that on normal cells [47]. Besides, a recent study has shown the membrane architecture differences between healthy and pathological cells [48]. Hence, investigating the fine topography of cell surface benefits better understanding cells. The different roughness of cell surfaces among the three types of cells (C2C12, HEK293, MCF-7) observed here may be associated with the different surface structures of cells. Besides, the cell membrane patches on substrates are the direct interface during cell growth, and therefore investigating membrane patches is useful for understanding the detailed situations about cell-substrate interactions. Studies have shown that the roughness of living macrophage cells is in the range of 10-200 nm [49], which is much larger than the roughness of cell membrane patches measured here. Living cells have a soft and fragile surface, which causes that AFM tip is prone to deform the cell membrane and sense the intracellular structures [50]. Thus, roughness extracted from AFM images of living cells is the convolution of cell surface and intracellular structures. Fig. 4E shows a cell membrane patch on which some hollow areas are discernible (denoted by the asterisk). For the hollow areas, we can clearly see the nanogranular structures on the substrate, directly indicating that cells grow on nanogranule-coated substrates. After performing mechanical scratching on the decellularized substrates with the use of micropipette, AFM images of the decellularized substrates were recorded, clearly showing that the nanogranular structures on the decellularized substrates have multiple layers (Fig. 4F). AFM section profile analysis shows that the height of scratching is typically about 4.5 nm and the width of scratching is often several hundred nanometers (Fig. S7). A notable point is that the scratching is associated with the force exerted on the micropipette tip and we can see the nanogranular structures in the groove caused by scratching (III, V in Fig. 4F), indicating that the micropipette tip did not touch the surface of bare glass slides but touched the nanogranular structures deposited on the substrates. Statistical measurements show that the top layer is much rougher than the bottom layer (VI in Fig. 4F).

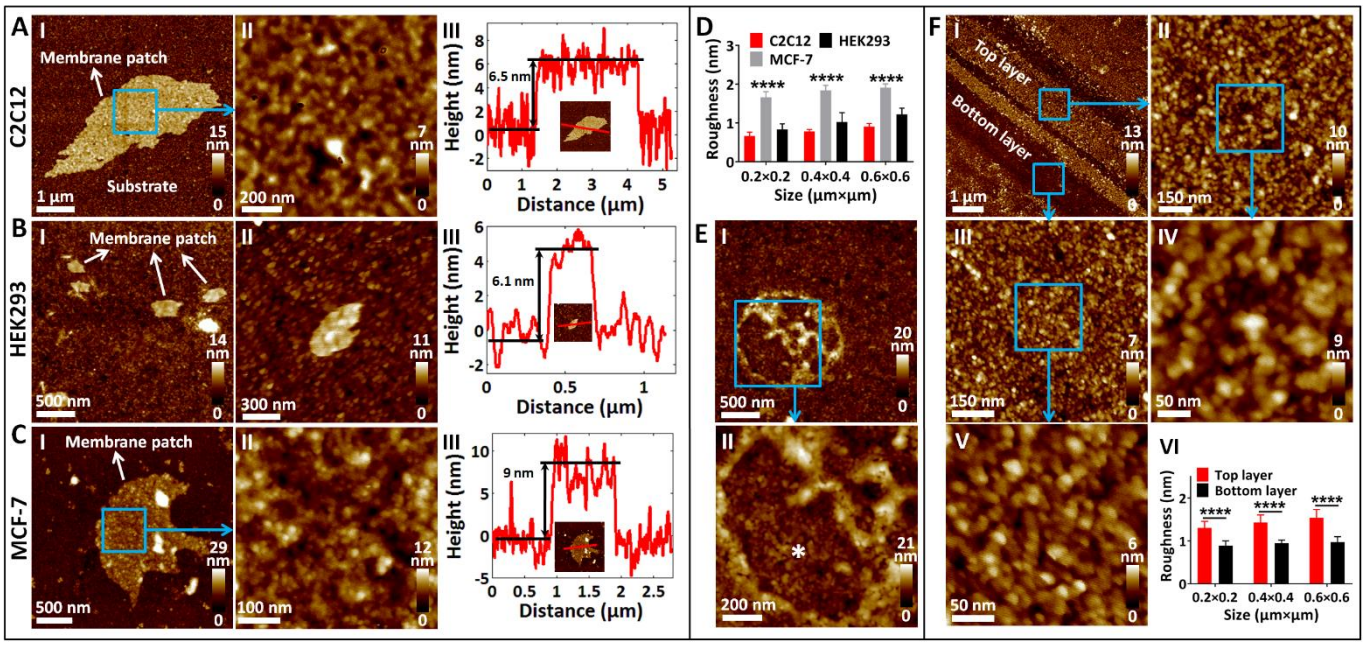

Figure 4 AFM imaging and roughness analysis of membrane patches and nanogranular layers on the decellularized substrates for revealing the detailed cell-substrate interface. AFM images were recorded in air. (A, B, C) Cell membrane patches left on the decellularized substrates. Decellularized substrates were obtained by treating the glass slides (cells were grown on glass slides) with trypsin for 1 min. (A) C2C12 cells, (B) HEK293 cells, and (C) MCF-7 cells. (I) Large-size scan images, (II) small-size scan images, and (III) section profile curves of the membrane patches taken along the red curves in the inset AFM images. (D) Surface roughness (Mean±SD) contrast of the cell membrane patches. (E) AFM images showing nanogranular structures beneath the cell membrane patches. (I) Large scan size imaging and (II) small scan size imaging. The asterisk denotes the hollow area of the membrane patch. (F) AFM images showing the multiple layers of the nanogranular structures on the decellularized substrates. AFM images were recorded after mechanically scratching the decellularized substrates with a micropipette. (I) AFM image of the whole scan area containing multiple layers of nanogranular structures. (II) Large-size scan imaging and (IV) small-size scan imaging of top layer. (III) Large-size scan imaging and (V) small-size scan imaging of bottom layer. (VI) Surface roughness (Mean±SD) contrast of top layer and bottom layer. N=50, *P<0.05; **p<0.01; ***p<0.001; ****p<0.0001.

AFM imaging reveals that nanogranular substances from cell culture medium deposit on substrates for promoting cell growth. AFM images of the non-cell areas of the glass slides (cells were grown on glass slides) also show the nanogranular structures (Fig. 5A, B and Fig. S8). Bare glass slides which were placed in cell culture medium without cells exhibit the nanogranular structures as well (Fig. 5C, D). Statistical analysis shows that bare glass slides without growing cells became significantly rougher when the incubation time increased from 24 h to 72 h (I in Fig. 5E), and this may due to the depositions of nanogranular structures on substrates from cell culture medium. For the glass slides growing cells, the roughness of non-cell area of the glass slides kept stable when the incubation time increased from 24 h to 72 h (II in Fig. 5E), and this may due to the depositions of nanogranular structures on substrates from cell culture medium and also the substances secreted from cells, indicating the effect of growing cells on substrate surface. Besides, freshly cleaved mica was placed in cell culture medium and incubated at 37℃(5%). Nanogranular structures are clearly observed from the obtained AFM images of the mica after incubation (Fig. S8). Freshly cleaved mica has a smooth surface (Fig. 1C), and thus we can conclude that the nanogranular structures on mica were from cell culture medium. The dynamic changes of substrate surface were visualized by AFM time-lapse imaging, clearly showing the appearance and accumulation of nanogranular structures on both glass slides (Fig. 5F) and mica (Fig. 5G). We can even see that once the substrate was placed in cell culture medium (in less than 1 min),

nanogranules attached onto the substrates (II in Fig. 5F, G). The attachment of nanogranules onto substrates was accompanied with the roughening of substrates (V in Fig. 5F, G). Further, in order to examine which components in cell culture medium contribute to the nanogranular depositions on substrates, AFM images of glass slides placed in diverse types of solutions which correspond to the different types of components in cell culture medium. Cell culture medium used here is DMEM medium containing 10% FBS and 1% penicillin-streptomycin solution. In order to split the different components of the cell culture DMEM solution, 10% FBS diluted by PBS, and 1% penicillin-streptomycin diluted by PBS were used. PBS was used for control. AFM images clearly show that nanogranular depositions are observed for the substrates placed in 10% FBS solution and DMEM solution (Fig. 6C, D), while no nanogranular depositions are observed for the substrates placed in PBS and 1% penicillin-streptomycin solution (Fig. 6A, B). The results indicate that nanogranular substances from FBS and DMEM solution are involved in the nanogranular depositions coated on the substrates. We then examined the effects of nanogranular depositions on substrates for cell growth. Cells were grown on cell culture medium-treated glass slides for 24 h and then optical and fluorescent images of cells were recorded (Fig. 7). AO staining fluorescent images were used to clearly visualize the cell nucleus for exactly identifying cell number after growth. The results (Fig. 7) show that on the whole cells grown on cell culture medium-treated glass slides proliferated faster than cells grown on bare glass slides (not treated by cell culture medium in advance), indicating that nanogranular depositions on substrates from cell culture medium promote cell growth. Taken together, the experimental results show that FBS and DMEM components are involved in the nanogranular depositions coated on substrates, which facilitate cell growth.

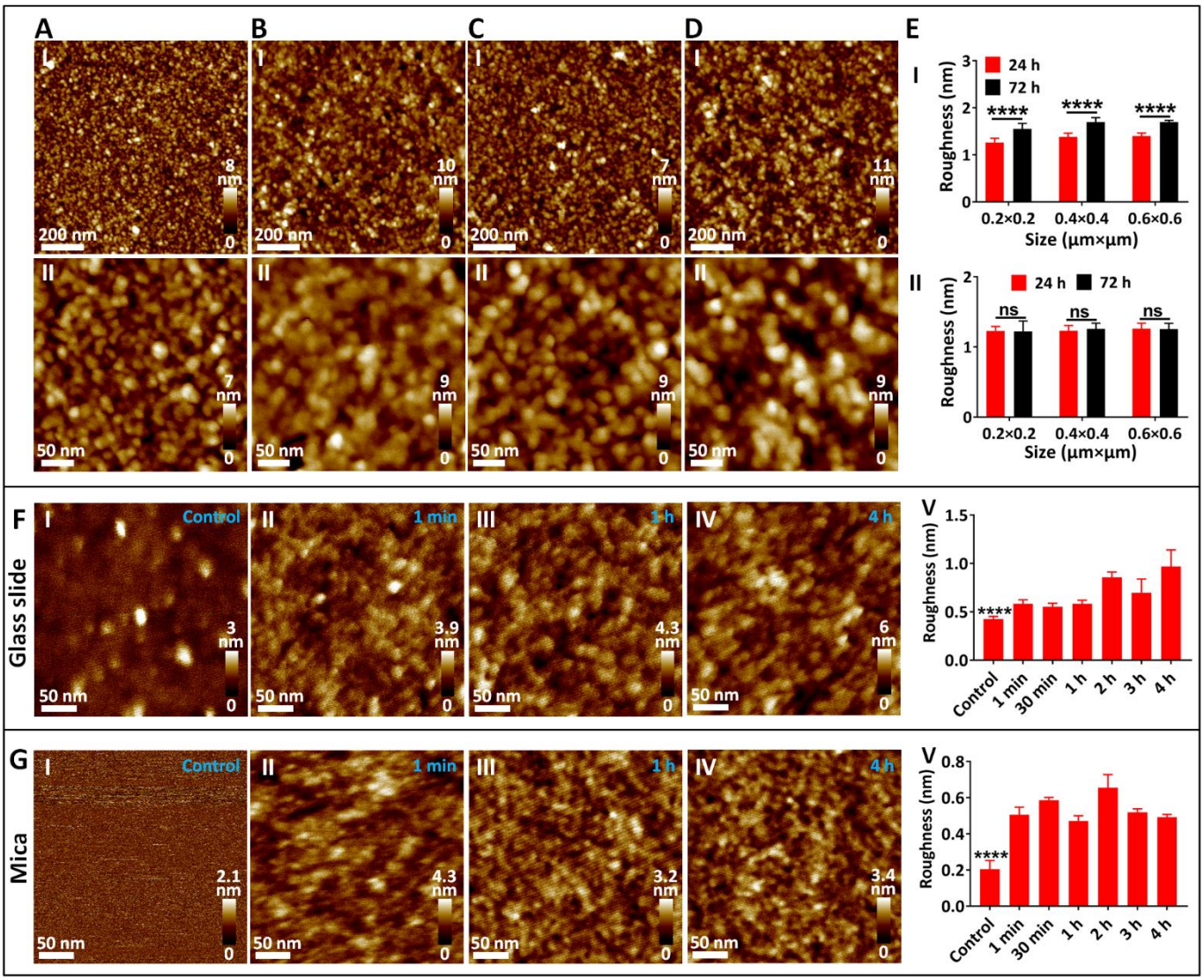

Figure 5 AFM time-lapse imaging revealing that cell culture medium contributes to the nanogranular biological depositions. AFM images were recorded in air. (A, B) AFM images of non-cell areas of glass slides after growing HEK293 cells for 24 h (A) and 72 h (B). (C, D) AFM images of bare glass slides after being placed in cell culture medium at 37℃(5%CO_2) for 24 h (C) and 72 h (D). (I) Large-size scan images and (II) small-size scan images. (E) Roughness (Mean±SD) changes of the glass slides. (I) Bare glass slides placed in cell culture medium without growing cells. (II) Non-cell areas of the glass slides growing HEK293 cells. (F, G) AFM time-lapse imaging revealing the real-time morphological dynamics of substrates. Bare substrates (glass slide or mica) were incubated in cell culture medium at 37℃(5%CO_2) for a certain time and then AFM images of the bare substrates were obtained. (F) Glass slides. (G) Mica. (I) Substrates before being placed in cell culture medium. (II) 1 min, (III) 1 h, and (IV) 4 h after placing the bare substrates into the cell culture medium and incubating at 37℃ (5%CO_2). (V) Roughness (Mean±SD) changes of the bare substrates. N=50, *P<0.05; **p<0.01; ***p<0.001; ****p<0.0001.

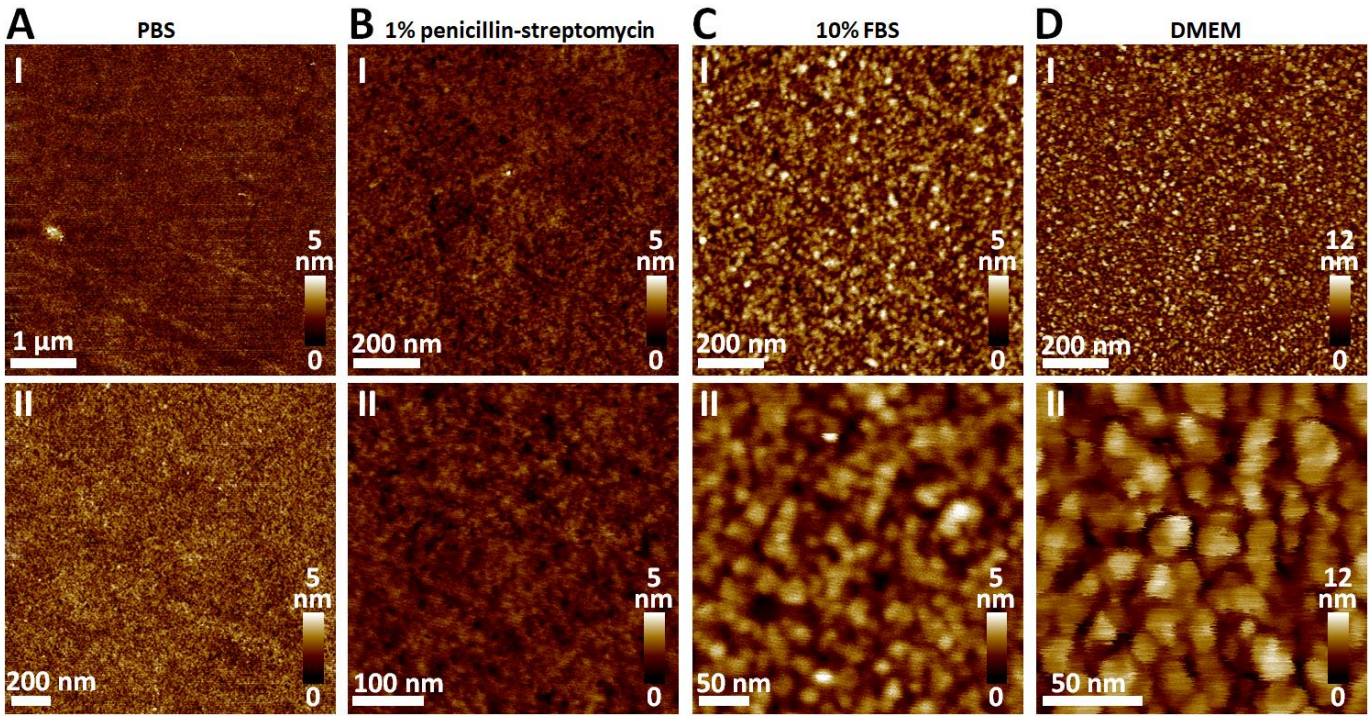

Figure 6 AFM imaging revealing the cell culture medium components which contribute to the nanogranular biological depositions on substrates. Glass slides were placed in various types of solutions corresponding to the different components of cell culture medium and incubated at 37℃(5%CO_2) for 24 h. After incubation, glass slides were washed by pure water and then imaged by AFM. AFM images were recorded in air. (A) PBS. (B) 1% penicillin-streptomycin solution diluted by PBS. (C) 10% FBS solution diluted by PBS. (D) DMEM solution. (I) Large-size scan images and (II) small-size scan images.

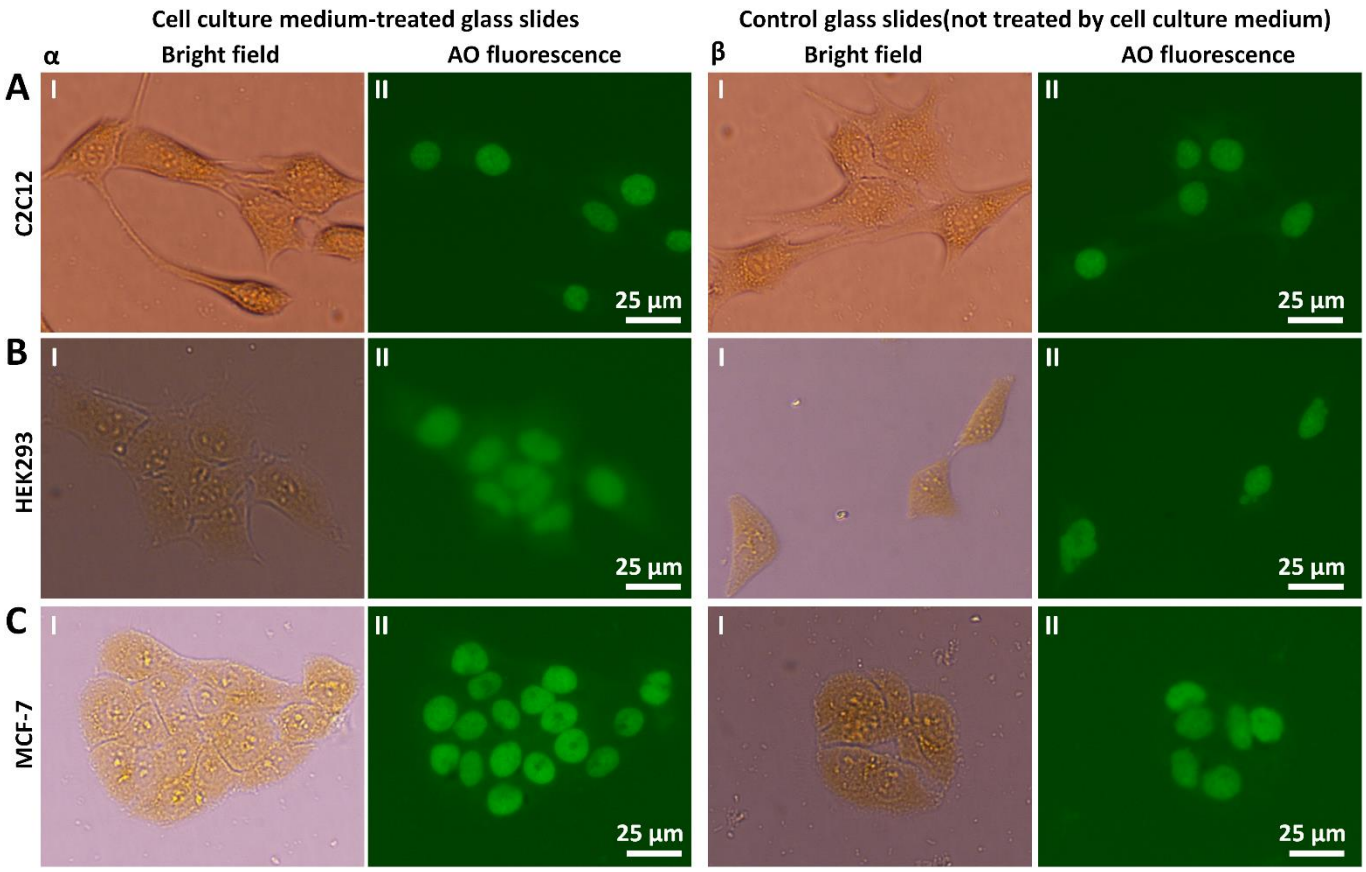

Figure 7 Nanogranular depositions on the substrates from cell culture medium promote cell growth. Cells were grown on two types of glass slides. One type of glass slides was previously placed in cell culture medium and incubated at 37℃(5%CO_2) for 24 h (α), and the other type of glass slides were regular glass slides which were not previously treated by cell culture medium (β). For both the two types of glass slides, cells were grown for 24 h at 37℃(5%CO_2) and then optical and fluorescent images of cells on the glass slides were recorded. (A) C2C12 cells. (B) HEK293 cells. (C) MCF-7 cells. (I) Bright field images and corresponding (II) fluorescence images. The AO dye is used to stain cells. Cells exhibit green fluorescence after being stained by AO dyes.

Utilizing AFM to image the fine structures of the substrates opens novel possibilities for the studies of nanoscopic cell-substrate interactions. Cell adhesion to the ECM is fundamental to tissue integrity and human health [51]. Cells adhere to the substrates *via* the adhesion molecules expressed on cell surface, particularly the integrin [52]. The extracellular domains of integrin bind to the ECM components (e.g., fibronectin, collagen, and other ECM proteins) and the cytoplasmic tails of integrin are linked to the actin cytoskeleton, which integrates cytoskeletal dynamics, cell adhesion and migration [53]. Three-dimensional super-resolution fluorescence microscopy has been utilized to investigate the nanoscale architecture of integrin-based cell adhesion [54], showing the molecular organization at the cellular focal adhesion areas. The nanotopography of the substrate has been shown to be able to regulate the fate of cells from the bottom [55]. Here, the results obtained by AFM imaging show that the substrates on which cells are grown considerably exhibits nanogranular structures (Fig. 2-Fig. 4). Besides, AFM images show that nanogranules from cell culture medium (particularly from FBS and DMEM) deposit on the substrates to involve in the constitution of ECM and promote cell growth (Fig. 5-Fig. 7). Studies have identified several types of proteins which are involved in FBS, including fibronectin, macroglobulin, ceruloplasmin, transferrin and albumin [56]. The deposition of the proteins on the substrates from FBS changes the surface free energy of substrates, which has been shown to influence cell growth [57]. Hence, further experiments, which utilize antibodies to identify the specific proteins deposited on the substrates and then correlate these proteins with the nanogranular structures observed by AFM, will be particularly useful

for understanding cell-substrate interactions. However, it should be noted that FBS contains many different ingredients and the compositions of FBS are still not fully understood so far [58, 59], which causes difficulties in completely revealing cell-substrate interactions. Besides, cells are able to secrete endogenous fibronectin proteins to coat the substrates for promoting cell growth [60], which adds the complexity of cell-substrate interactions. Altogether, the results show that AFM is able to resolve the nanogranular structures of the substrates with unprecedented spatial resolution for cell growth, which improves our understanding of the ECM and will facilitate investigating the underlying mechanisms guiding cell-substrate interactions.

3.3 Structural and mechanical dynamics of substrates and cells during cell growth

AFM imaging reveals the surface alterations of substrates after growing cells. In order to examine the effect of cell growth on the substrates, AFM images were recorded at the non-cell areas of the three types of substrates (glass slide, mica, Petri dish) after growing cells on the substrates, as shown in Fig. 8. AFM images clearly show the nanogranular structures on the substrates (I, II, III in Fig. 8A-C). For glass slides and mica, roughness analysis shows that substrates growing C2C12 cells were significantly smoother than the substrates grew MCF-7 cells and HEK293 cells (IV in Fig. 8A, B). However, the Petri dishes growing MCF-7 cells were significantly rougher than that growing C2C12 cells or HEK293 cells (IV in Fig. 8C). The roughness of the bare substrates (glass slide, mica, Petri dish) without growing cells was shown in Fig. 1 and Fig. S4, confirming the roughening of substrates after growing cells. ECM is composed of a large collection of biochemically distinct components including proteins, glycoproteins, proteoglycans, and polysaccharides [9]. During cell growth, cells secrete ECM components to facilitate their adhesion and the subsequent proliferation on the substrate. For example, studies have shown that human glial tumor cells secrete various ECM compositions (including laminin, fibronectin, vitronectin, and thrombospondin) during the cellular attachments to substratum [61]. Particularly, the ECM components secreted by different cells (e.g., normal cells and cancerous cells) often exhibit different structural and mechanical properties [62-64]. In addition, nanogranules from cell culture medium also attach to the substrates (Fig.5). Therefore, the attachments of cell-secreted ECM components and cell culture medium nanogranules might cause the different topographical characteristics of the substrates after growing different types of cells.

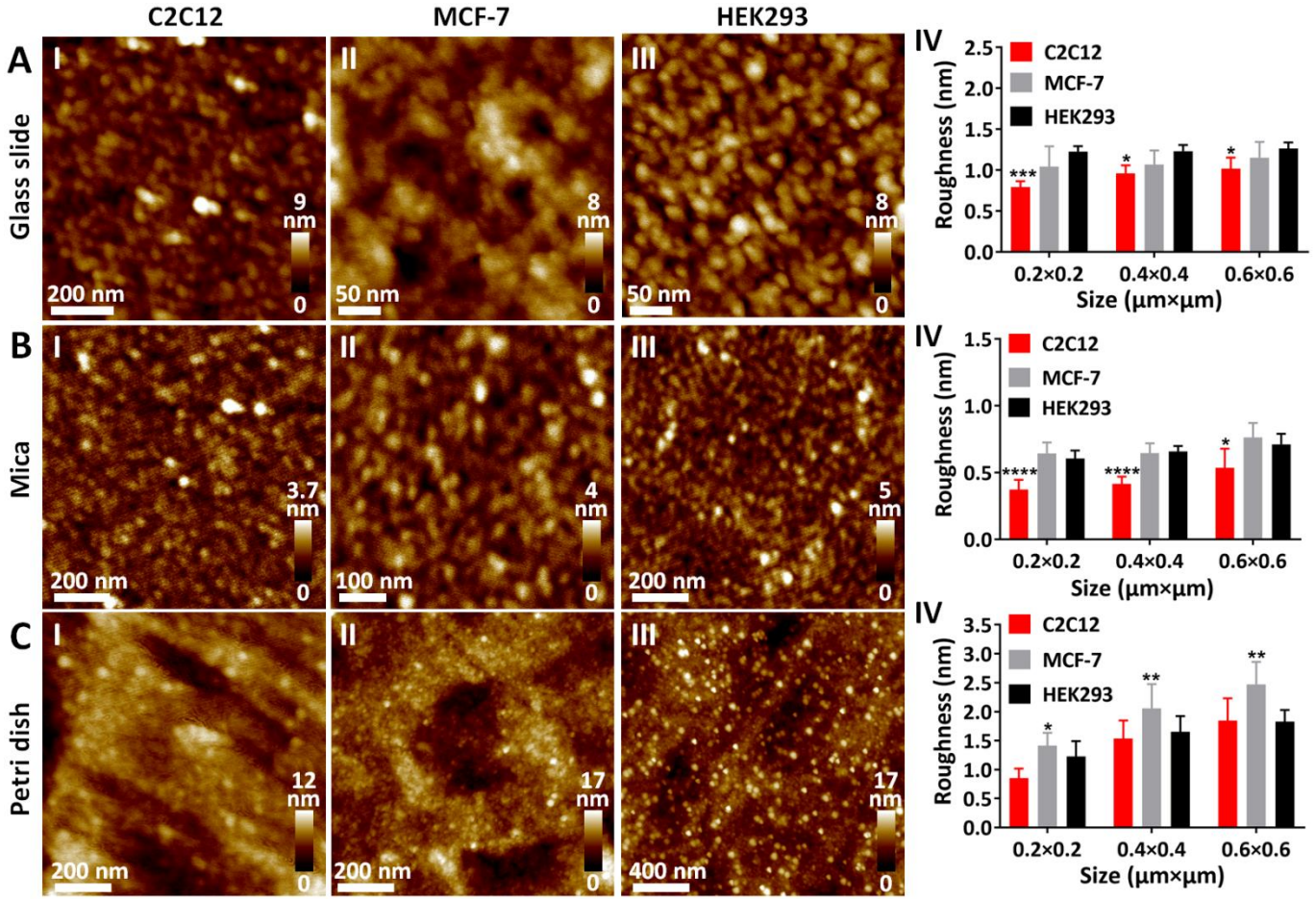

Figure 8 AFM imaging and roughness changes of the substrates after growing cells. The non-cell areas of the substrates (cells were grown on the substrates) were imaged by AFM. AFM images were recorded in air. (A) Glass slide. (B) Mica. (C) Petri dish. (I, II, III) AFM images of the non-cell areas of the substrates growing C2C12 cells (I), MCF-7 cells (II) or HEK293 cells (III). (IV) Surface roughness (Mean±SD) statistics of the substrates after growing cells. N=50, *P<0.05; **p<0.01; ***p<0.001; ****p<0.0001.

AFM mechanical measurement reveals the diverse adhesion forces of cells cultured on different types of substrates. Under the guidance of optical microscopy (Fig. S9), AFM probes were moved to the living cells cultured on substrates (glass slide, mica, or Petri dish) and then force curves were obtained on the cells. By analyzing the retract curves of the force curves obtained on living cells, the adhesion forces between cells and AFM tips are measured. From the retract curves, two types of the molecular unbinding events are significantly observed (Fig. 9C), including the unbinding of membrane receptors which do not anchor the cytoskeleton and the unbinding of membrane receptors which anchor the cytoskeleton [65-67]. Typical force curves obtained on cells cultured on different substrates are shown in Fig. 10. From the statistical histograms of adhesion forces (IV in Fig. 10), we can see that for all of the three substrates (glass slide, mica, and Petri dish) the adhesion forces of MCF-7 cells are significantly larger than that of C2C12 cells and HEK293 cells. Besides, the adhesion forces of MCF-7 cells cultured on glass slide are much smaller than the adhesion forces of MCF-7 cells cultured on mica and Petri dish. For C2C12 cells and HEK293 cells, the cellular adhesion forces also vary when they are cultured on different substrates. Cell adhesion characteristics plays an important role in regulating the behaviors and biological functions of cells. Abnormal cytoadherence capability is often associated with the pathological changes [68], such as cancer metastasis [69] and cardiovascular disease [70]. Therefore, cancerous cells (MCF-7) and normal cells (C2C12 and HEK293) may exhibit different adhesion forces. Besides, the three types of substrates used here have different surface topographical features (mica surface is smoothest while dish surface is roughest, as shown in Fig. 1 and Fig. S4) and the cell types are different from each other, which may cause that the adhesion

forces of cells are diverse when cells are grown on different substrates.

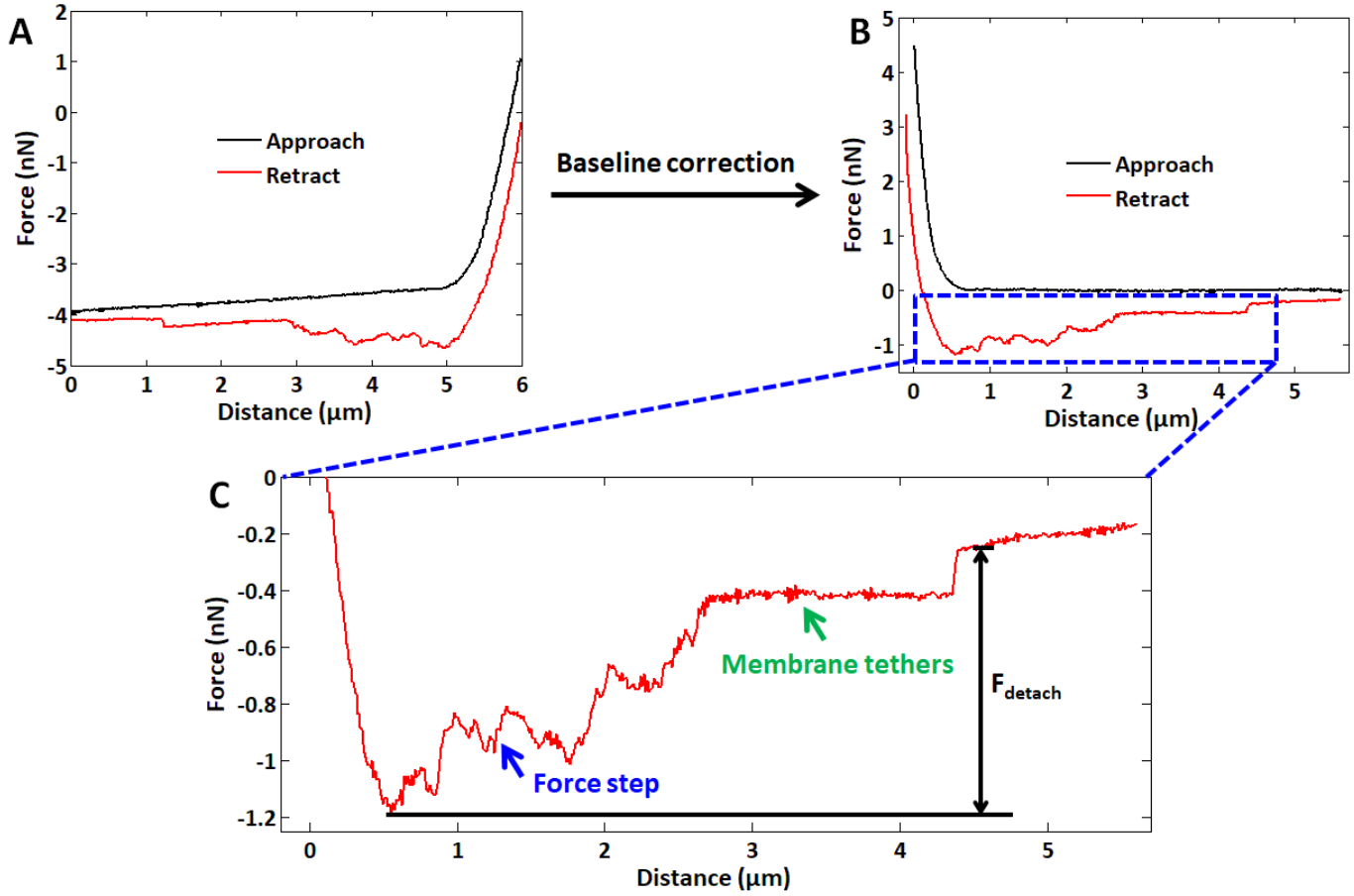

Figure 9 Typical force curves with adhesion force peaks obtained on living cells in cell culture medium. (A) An original force curve. (B) The force curve after performing baseline correction with the use of AFM offline software Nanoscope Analysis (Bruker, Santa Barbara, CA, USA). (C) The amplifying plot of the retract curve (denoted by the dashed square in B). Two types of molecular unbinding events are observed from the retract curve, including the unbinding of membrane receptors which do not anchor the cytoskeleton (denoted by the green arrow) and the unbinding of membrane receptors which anchor the cytoskeleton (denoted by the blue arrow). The adhesion force (F_{detach}) is defined as the maximum downward force exerted on the cantilever of AFM.

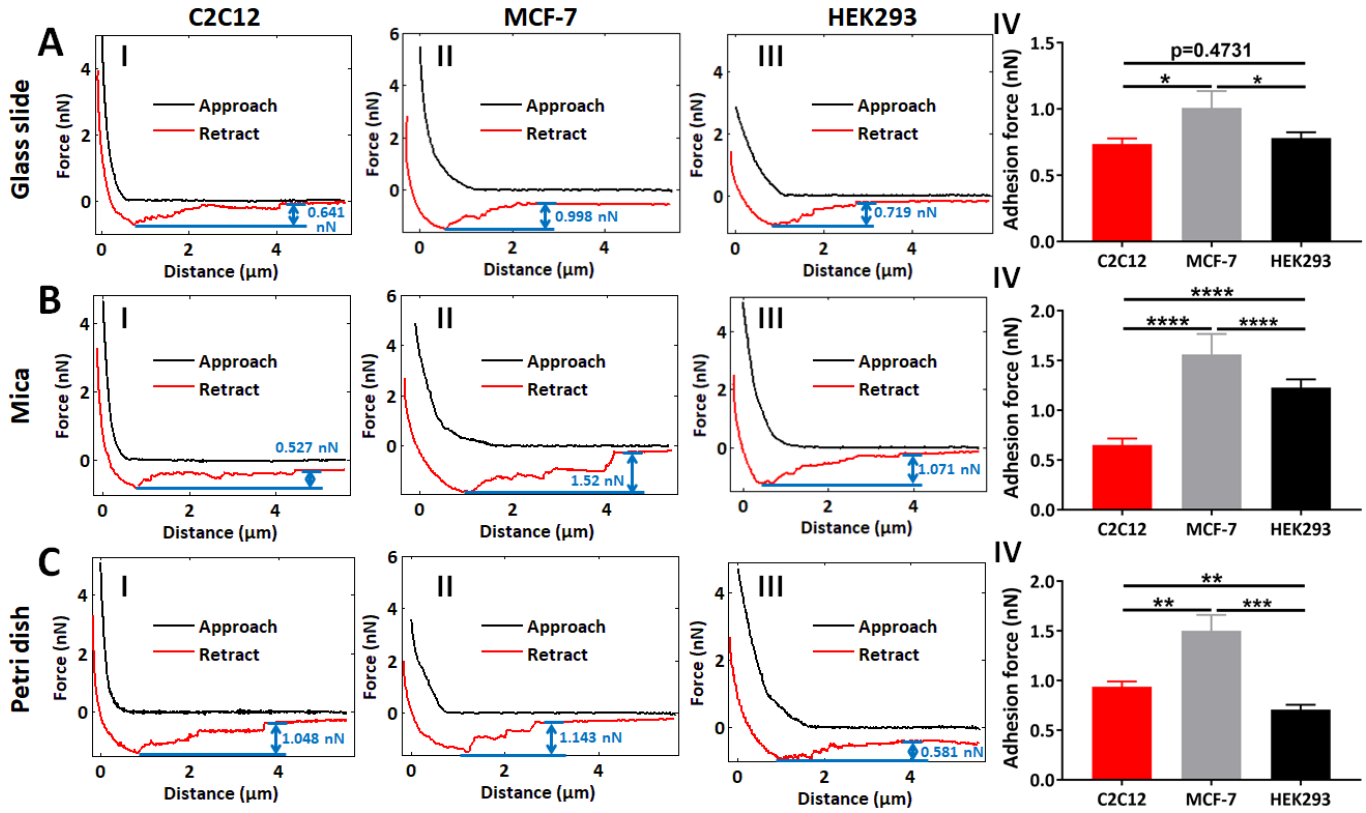

Figure 10 Measuring the adhesion forces of cells cultured on different types of substrates by AFM in cell culture medium. (A, B, C) Cells grown on glass slide (A), mica (B), or Petri dish (C). (I, II, III) Typical force curves obtained on C2C12 cells (I), MCF-7 cells (II) or HEK293 cells (III). (IV) Statistics of cellular adhesion forces (Mean±SEM) on different substrates. The blue arrows denote the adhesion forces calculated from the retract curves. N=50, *P<0.05; **p<0.01; ***p<0.001; ****p<0.0001.

Effects of substrates on the elastic and viscoelastic behaviors of cells are revealed by AFM. During the process of controlling AFM tip to perform approach-dwell-retract process on living cells in the vertical direction, two types of curves are recorded, including force-distance (F-D) curves and force-time (F-T) curves. The F-D curves are used for analyzing cellular elastic properties, whereas F-T curves are used for analyzing cellular viscoelastic properties [25, 29]. Fig. 11AI shows a typical F-D curve, which includes two portions, including an approach curve and a retract curve. Fitting the indentation curve with Hertz-Sneddon model yields the cellular Young's modulus [71, 72] (shown in the inset in Fig. 11AI and Fig. S10), showing that the experimental indentation curve is consistent with the theoretical fitting curve. Fig. 10AII shows a typical F-T curve obtained on cells. Fitting the F-T curve with two-order Maxwell model yields two cellular relaxation times (shown in the inset in Fig. 11AII and Fig. S11), showing that the experimental indentation curve is in agreement with the theoretical fitting curve. From the statistical histograms, we can see that the Young's modulus of C2C12 cells is significantly larger than that of HEK293 cells and MCF-7 cells except for mica (I in Fig. 11B-D). Besides, the cellular Young's modulus changed when cells were grown on different substrates, indicating the influence of growth substrate on cellular elasticity. For cellular relaxation times, on the whole there are no significant differences for the three types of cells (II, III in Fig. 11B-D), but cells cultured on different types of substrates exhibit diverse cellular relaxation time τ_1. Cell mechanics has been shown to be an important indicator which tightly links cell structures and cell functions [73, 74]. Mechanical changes of cells are often accompanied with the physiological or pathological changes of cells, for example cancerous cells are commonly softer than their normal counterparts [75, 76]. Here, the different cellular Young's modulus between cells may due to the fact that the cells are from different origins (MCF-7 cells are from breast tissue, HEK293 cells are from kidney, and C2C12 cells are myoblasts). For the

three types of cells grown on different substrates, the cellular Young's modulus exhibits uniform changes, indicating the influence of substrates (e.g., substrate surface features) on cellular elasticity. On the contrast, the cellular viscoelastic properties exhibit various changes for different types of cells in response to the substrates, indicating the diverse effects of substrates on the viscoelastic behaviors of cells.

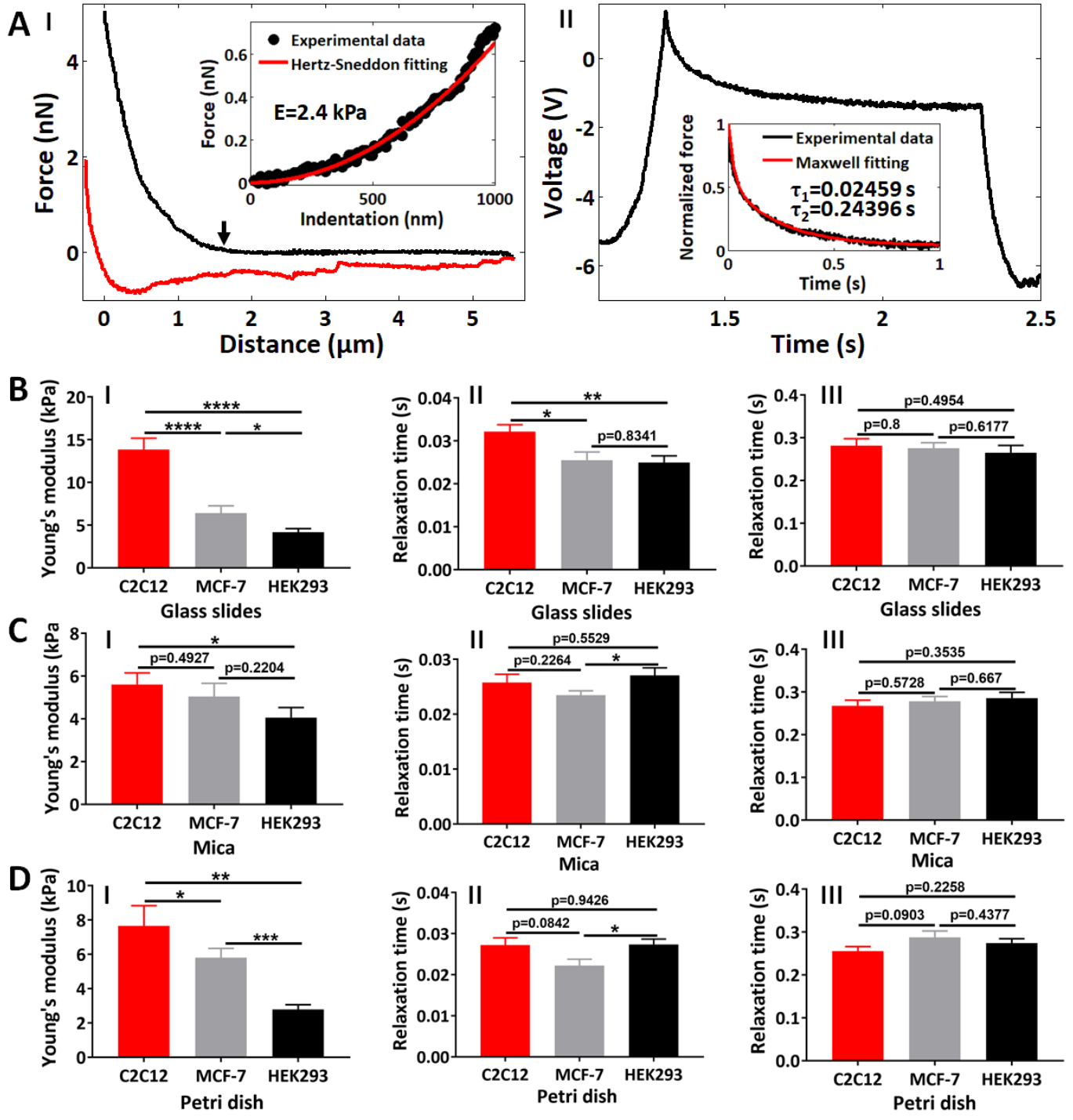

Figure 11 Measuring the elastic and viscoelastic properties of cells cultured on different types of substrates by AFM in cell culture medium. (A) Measuring the Young's modulus (I) and relaxation time (II) of cells by AFM. (I) Extracting cellular Young's modulus from the approach curve of the force curve. The black curve corresponds to approach curve and the red curve corresponds to retract curve. The black arrow denotes the contact point in the approach curve. According to the contact point, the approach curve is converted into the indentation curve. The inset shows the comparison between experimental indentation curve and theoretical fitting curve. (II) Extracting cellular relaxation times from the relaxation curves. The inset shows the comparison between experimental relaxation curve and theoretical fitting curve. (B-D) Statistical cellular mechanical properties (Mean±SEM) measured on the cells grown on glass slide (B), mica (C), or Petri dish (D). (I)

Cellular Young's modulus. (II) Cellular relaxation time τ_1. (III) Cellular relaxation time τ_2. N=50, *P<0.05; **p<0.01; ***p<0.001; ****p<0.0001.

The experimental results revealed by AFM from visualizing the fine structures of cell-substrate interface and probing the mechanical properties of cells will potentially benefit the studies of cellular behaviors. First, the regulatory role of substrates on cell functions has been largely investigated from the structures and properties of substrates. The nanoscale geometry and size of the features of the ECM have significant effects on various cell behaviors, such as attachment/adhesion, migration, and proliferation, but the mechanisms responsible for these effects are poorly understand [77]. The cell/material interface is a complex, dynamic microenvironment in which the cell and the material cooperatively dictate one another's fate [78]. A recent study by Mpoyi et al [79] has shown that protein adsorption on the substrates is a key mediator in the nanotopographical control of cell behavior. Here, our results obtained by AFM high-resolution imaging clearly show that nanogranules from cell culture medium attach onto the substrate to form nanogranular topography for promoting cell growth. To the best of our knowledge, the results are previously unrecognized and thus provide novel insights into the regulatory role of substrates for cellular behaviors at the nanoscale. Second, interactions between cells and ECM may cause the alterations of cellular functions [80], which are often accompanied with the changes of cellular structures (such as cytoskeletons [81]) and cellular mechanical properties, such as adhesion force, elasticity, and viscoelasticity [82]. Hence, investigations of cell mechanics on substrates with different surface features are meaningful to examine the role of physical interactions and mechanical forces [83] in pathological processes for guiding cellular behaviors.

4. Conclusions

This work has demonstrated the outstanding capabilities of AFM in observing the detailed situations of cell-substrate interactions at the nanoscale on three different types of substrates (glass slide, mica, Petri dish) with the use of three different types of cells (C2C12, HEK293, MCF-7). AFM images of decellularized substrates prepared by ammonia or trypsin significantly reveal the nanogranular topography of the substrates on which cells grow, while AFM images of native substrates prove that nanogranules from cell culture medium (particularly from FBS and DMEM solution) contribute to the nanogranular depositions on the substrates to promote cell growth, which are previously undiscovered and improve our understanding of cell-substrate interactions. AFM imaging and mechanical measurements reveal the dynamic changes of substrate topography and cell mechanics during cell growth, showing the diverse impacts of cell-substrate interactions on substrates and cells. The established methods here can be applied to other types of biological and biomaterial systems, which is therefore with generally fundamental significance. Taken together, this study provides a novel method based on AFM to investigate nanotopographical cues for cell-substrate interactions from visualizing substrate fine structures to characterizing surface roughness as well as single-cell mechanical analysis, which will be particularly useful for uncovering the underlying mechanisms guiding cellular behaviors.

Acknowledgements

This work was supported by the National Natural Science Foundation of China (61922081, 61873258, U1613220) and the Youth Innovation Promotion Association Chinese Academy of Sciences (2017243).

Supplementary information

Extracting surface roughness of substrates, measuring cellular relaxation times, AFM images, size analysis of nanogranules, roughness of bare substrates, optical images, experimental curves, and theoretical fittings

References

[1] Junttila, M. R.; de Sauvage, F. J. Influence of tumour micro-environment heterogeneity on therapeutic response. *Nature* **2013**, *501* (7467), 346-354. DOI: 10.1038/nature12626

[2] Sun, Y.; Chen, C. S.; Fu, J. Forcing stem cells to behave: a biophysical perspective of the cellular microenvironment. *Ann. Rev. Biophys.* **2012**, *41*, 519-542. DOI: 10.1146/annurev-biophys-042910-155306

[3] Frantz, C.; Stewart, K. M.; Weaver, V. M. The extracellular matrix at a glance. *J. Cell Sci.* **2010**, *123* (24), 4195-4200. DOI: 10.1242/jcs.023820

[4] Hoffman, B. D.; Grashoff, C.; Schwartz, M. A. Dynamic molecular processes mediate cellular mechanotransduction. *Nature* **2011**, *475* (7356), 316-323. DOI: 10.1038/nature10316

[5] Gauthier N. C.; Roca-Cusachs, P. Mechanosensing at integrin-mediated cell-matrix adhesions: from molecular to integrated mechanisms. *Curr. Opin. Cell Biol.* **2018**, *50*, 20-26. DOI: 10.1016/j.ceb.2017.12.014

[6] Wang, N.; Tytell, J. D.; Ingber, D. E. Mechanotransduction at a distance: mechanically coupling the extracellular matrix with the nucleus. *Nat. Rev. Mol. Cell Biol.* **2009**, *10* (1), 75-82. DOI: 10.1038/nrm2594

[7] Wang, N. Review of cellular mechanotransduction. *J. Phys. D Appl. Phys.* **2017**, *50* (23), 233002. DOI: 10.1088/1361-6463/aa6e18

[8] Garcia, J. R.; Garcia, A. J. Cellular mechanotransduction: sensing rigidity. *Nat. Mater.* **2014**, *13* (6), 539-540. DOI: 10.1038/nmat3996

[9] Lu, P.; Weaver, V. M.; Werb, Z. The extracellular matrix: a dynamic niche in cancer progression. *J. Cell Biol.* **2012**, *196* (4), 395-406. DOI: 10.1083/jcb.201102147

[10] Spill, F.; Reynolds, D. S.; Kamm, R. D.; Zaman, M. H. Impact of the physical microenvironment on tumor progression and metastasis. *Curr. Opin. Biotechnol.* **2016**, *40*, 41-48. DOI: 10.1016/j.copbio.2016.02.007

[11] Mitchell, M. J.; Jain, R. K.; Langer, R. Engineering and physical sciences in oncology: challenges and opportunities. *Nat. Rev. Cancer* **2017**, *17* (11), 659-675. DOI: 10.1038/nrc.2017.83

[12] Chaudhuri, P. K.; Low, B. C.; Lim, C. T. Mechanobiology of tumor growth. *Chem. Rev.* **2018**, *118* (14), 6499-6515. DOI: 10.1021/acs.chemrev.8b00042

[13] Watt, F. M.; Huck, W. T. S. Role of the extracellular matrix in regulating stem cell fate. *Nat. Rev. Mol. Cell Biol.* **2013**, *14* (8), 467-473. DOI: 10.1038/nrm3620

[14] Klim, J. R.; Li, L.; Wrighton, P. J.; Piekarczyk, M. S.; Kiessling, L. L. A defined glycosaminoglycan-binding substratum for human pluripotent stem cells. *Nat. Methods* **2010**, *7* (12), 989-994. DOI: 10.1038/nmeth.1532

[15] Seliktar, D. Designing cell-compatible hydrogels for biomedical applications. *Science* **2012**, *336* (6085), 1124-1128. DOI: 10.1126/science.1214804

[16] Lutolf, M. P.; Gilbert, P.M.; Blau, H. M. Designing materials to direct stem-cell fate. *Nature* **2009**, *462* (7272), 433-441. DOI: 10.1038/nature08602

[17] Higuchi, A.; Ling, Q. D.; Chang, Y.; Hsu, S.T.; Umezawa, A. Physical cues of biomaterials guide stem cell differentiation fate. *Chem. Rev.* **2013**, *113* (5), 3297-3328. DOI: 10.1021/cr300426x

[18] Li, Y.; Xiao, Y.; Liu, C. The horizon of materiobiology: a perspective on material-guided cell behaviors and tissue engineering. *Chem. Rev.* **2017**, *117* (5), 4376-4421. DOI: 10.1021/acs.chemrev.6b00654

[19] Caliari, S. R.; Burdick, J. A. A practical guide to hydrogels for cell culture. *Nat. Methods* **2016**, *13* (5), 405-414. DOI: 10.1038/nmeth.3839

[20] Dalby, M. J.; Gadegaard, N.; Oreffo, R. O. C. Harnessing nanotopography and integrin-matrix interactions to influence stem cell fate. *Nat. Mater.* **2014**, *13* (6), 558-569. DOI: 10.1038/nmat3980

[21] Gu, L.; Mooney, D. J. Biomaterials and emerging anticancer therapeutics: engineering the microenvironment. *Nat. Rev. Cancer* **2016**, *16* (1), 56-66. DOI: 10.1038/nrc.2015.3

[22] Uto, K.; Tsui, J. H.; DeForest, C.A.; Kim, D. H. Dynamically tunable cell culture platforms for tissue engineering and mechanobiology. *Prog. Polym. Sci.* **2017**, *65*, 53-82. DOI: 10.1016/j.progpolymsci.2016.09.004

[23] Dufrene, Y. F.; Ando, T.; Garcia, R.; Alsteens, D.; Martinez-Martin, D.; Engel, A.; Gerber, C.; Muller, D. J. Imaging modes of atomic force microscopy for application in molecular and cell biology. *Nat. Nanotechnol.* **2017**, *12* (4), 295-307. DOI: 10.1038/nnano.2017.45

[24] Alsteens, D.; Gaub, H. E.; Newton, R.; Pfreundschuh, M.; Gerber, C.; Muller, D. J. Atomic force microscopy-based characterization and design of biointerfaces. *Nat. Rev. Mater.* **2017**, *2*, 17008. DOI: 10.1038/natrevmats.2017.8

[25] Li, M.; Liu, L.; Xiao, X.; Xi, N.; Wang, Y. Viscoelastic properties measurement of human lymphocytes by atomic force microscopy based on magnetic beads cell isolation. *IEEE Trans. Nanobiosci.* **2016**, *15* (5), 398-411. DOI: 10.1109/TNB.2016.2547639

[26] Lekka, M. Discrimination between normal and cancerous cells using AFM. *Bionanoscience* **2016**, *6* (1), 65-80. DOI: 10.1007/s12668-016-0191-3

[27] Li, M.; Liu, L.; Xu, X.; Xing, X.; Dang, D.; Xi, N.; Wang, Y. Nanoscale characterization of dynamic cellular viscoelasticity by atomic force microscopy with varying measurement parameters. *J. Mech. Behav. Biomed. Mater.* **2018**, *82*, 193-201. DOI: 10.1016/j.jmbbm.2018.03.036

[28] Li, M.; Xiao, X.; Liu, L.; Xi, N.; Wang, Y. Nanoscale quantifying the effects of targeted drug on chemotherapy in lymphoma treatment using atomic force microscopy. *IEEE Trans. Biomed. Eng.* **2016**, *63* (10), 2187-2199. DOI: 10.1109/TBME.2015.2512924

[29] Li, M.; Dang, D.; Liu, L.; Xi, N.; Wang, Y. Atomic force microscopy in characterizing cell mechanics for biomedical applications: a review. *IEEE Trans. Nanobiosci.* **2017**, *16* (6), 523-540. DOI: 10.1109/TNB.2017.2714462

[30] Rotsch, C.; Jacobson, K.; Radmacher, M. Dimensional and mechanical dynamics of active and stable edges in motile fibroblasts investigated by using atomic force microscopy. *Proc. Natl. Acad. Sci. USA* **1999**, *96* (3), 921-926. DOI: 10.1073/pnas.96.3.921

[31] Gavara, N.; Chadwick, R. S. Determination of the elastic moduli of thin samples and adherent cells using conical atomic force microscope tips. *Nat. Nanotechnol.* **2012**, *7* (11), 733-736. DOI: 10.1038/nnano.2012.163

[32] Kasas, S.; Longo, G.; Dietler, G. Mechanical properties of biological specimens explored by atomic force microscopy. *J. Phys. D Appl. Phys.* **2013**, *46* (13), 133001. DOI: 10.1088/0022-3727/46/13/133001

[33] Crapo, P. M.; Gilbert, T. W.; Badylak, S. F. An overview of tissue and whole organ decellularization processes. *Biomaterials* **2011**, *32* (12), 3233-3243. DOI: 10.1016/j.biomaterials.2011.01.057

[34] Lin, H.; Yang, G.; Tan, J.; Tuan, R. S. Influence of decellularized matrix derived from human mesenchymal stem cells on their proliferation, migration and multi-lineage differentiation potential. *Biomaterials* **2012**, *33* (18), 4480-4489. DOI: 10.1016/j.biomaterials.2012.03.012

[35] Lu, H.; Hoshiba, T.; Kawazoe, N.; Chen, G. Comparison of decellularization techniques for preparation of extracellular matrix scaffolds derived from three-dimensional cell culture. *J. Biomed. Mater. Res. A* **2012**, *100* (9), 2507-2516. DOI: 10.1002/jbm.a.34150

[36] Sart, S.; Ma, T.; Li, Y. Extracellular matrices decellularized from embryonic stem cells maintained their structure and signaling specificity. *Tissue Eng. Part A* **2014**, *20* (1-2), 54-66. DOI: 10.1089/ten.TEA.2012.0690

[37] Hoshiba, T.; Lu, H.; Kawazoe, N.; Chen, G. Decellularized matrices for tissue engineering. *Expert Opin. Biol. Ther.* **2010**, *10* (12), 1717-1728. DOI: 10.1517/14712598.2010.534079

[38] Rianna, C.; Kumar, P.; Radmacher, M. The role of the microenvironment in the biophysics of cancer. *Semin. Cell Dev. Biol.* **2018**, *73*, 107-114. DOI: 10.1016/j.semcdb.2017.07.022

[39] Uygun, B. E.; Soto-Gutierrez, A.; Yagi, H.; Izamis, M. L.; Guzzardi, M. A.; Shulman, C.; Milwid, J.; Kobayashi, N.; Tilles, A.; Berthiaume, F.; Hertl, M.; Nahmias, Y.; Yarmush, M. L.; Uygun, K. Organ reengineering through development of a transplantable recellularized liver graft using decellularized liver matrix. *Nat. Med.* **2010**, *16* (7), 814-820. DOI: 10.1038/nm.2170

[40] Song J. J.; Ott, H. C. Organ engineering based on decellularized matrix scaffolds. *Trends Mol. Med.* **2011**, *17* (8), 424-432. DOI: 10.1016/j.molmed.2011.03.005

[41] Shevach, M.; Fleischer, S.; Shapira, A.; Dvir, T. Gold nanoparticle-decellularized matrix hybrids for cardiac tissue engineering. *Nano Lett.* **2014**, *14* (10), 5792-5796. DOI: 10.1021/nl502673m

[42] Klaas, M.; Kangur, T.; Viil, J.; Maemets-Allas, K.; Minajeva, A.; Vadi, K.; Antsov, M.; Lapidus, N.; Jarvekulg, M.; Jaks, V. The alterations in the extracellular matrix composition guide the repair of damaged liver tissue. *Sci. Rep.* **2016**, *6*, 27398. DOI: 10.1038/srep27398

[43] Chen, W.C.; Wang, Z.; Missinato, M. A.; Park, D. W.; Long, D. W.; Liu, H. J.; Zeng, X.; Yates, N.A.; Kim, K.; Wang, Y. Decellularized zebrafish cardiac extracellular matrix induces mammalian heart regeneration. *Sci. Adv.* **2016**, *2* (11), e1600844. DOI: 10.1126/sciadv.1600844

[44] Damania, A.; Kumar, A.; Teotia, A. K.; Kimura, H.; Kamihira, M.; Ijima, H.; Sarin, S. K.; Kumar, A. Decellularized liver matrix-modified cryogel scaffolds as potential hepatocyte carriers in bioartificial liver support systems and implantable liver constructs. *ACS Appl. Mater. Interfaces* **2018**, *10* (1), 114-126. DOI: 10.1021/acsami.7b13727

[45] Hochmuth, R. M.; Evans, C. A.; Wiles, H. C.; McCown, J. T. Mechanical measurement of red cell membrane thickness. *Science* **1983**, *220* (4592), 101-102. DOI: 10.1126/science.6828875

[46] Paszek, M.J.; DuFort, C. C.; Rossier, O.; Bainer, R.; Mouw, J. K.; Godula, K.; Hudak, J. E.; Lakins, J. N.; Wijekoon, A. C.; Cassereau, L.; Rubashkin, M. G.; Magbanua, M. J.; Thorn, K. S.; Davidson, M. W.; Rugo, H. S.; Park, J. W.; Hammer, D. A.; Giannone, G.; Bertozzi, C. R.; Weaver, V. M. The cancer glycocalyx mechanically primes integrin-mediated growth and survival. *Nature* **2014**, *511* (7509), 319-325. DOI: 10.1038/nature13535

[47] Iyer, S.; Gaikwad, R. M.; Subba-Rao, V.; Woodworth, C. D.; Sokolov, I. Atomic force microscopy detects differences in the surface brush of normal and cancerous cells. *Nat. Nanotechnol.* **2009**, *4* (6), 389-393. DOI: 10.1038/nnano.2009.77

[48] Dumitru, A. C.; Poncin, M. A.; Conrard, L.; Dufrene, Y. F.; Tyteca, D.; Alsteens, D. Nanoscale membrane architecture of healthy and pathological red blood cells. *Nanoscale Horz.* **2018**, *3* (3), 293-304. DOI: 10.1039/C7NH00187H

[49] Li, M.; Liu, L.; Xi, N.; Wang, Y.; Xiao, X.; Zhang, W. Nanoscale imaging and mechanical analysis of Fc receptor-mediated macrophage phagocytosis against cancer cells. *Langmuir* **2014**, *30* (6), 1609-1621. DOI: 10.1021/la4042524

[50] Muller, D. J.; Dufrene, Y. F. Force nanoscopy of living cells. *Curr. Biol.* **2011**, *21* (6), R212-R216. DOI: 10.1016/j.cub.2011.01.046

[51] Hamidi, H.; Ivaska, J. Every step of the way: integrins in cancer progression and metastasis. *Nat. Rev. Cancer* **2018**, *18*

(9), 533-548. DOI: 10.1038/s41568-018-0038-z

[52] Desgrosellier, J. S.; Cheresh, D. A. Integrins in cancer: biological implications and therapeutic opportunities. *Nat. Rev. Cancer* **2010**, *10* (1), 9-22. DOI: 10.1038/nrc2748

[53] Parsons, J. T.; Horwitz, A. R.; Schwartz, M.A. Cell adhesion: integrating cytoskeletal dynamics and cellular tension. *Nat. Rev. Mol. Cell Biol.* **2010**, *11* (9), 633-643. DOI: 10.1038/nrm2957

[54] Kanchanawong, P.; Shtengel, G.; Pasapera, A. M.; Ramko, E. B.; Davidson, M. W.; Hess, H. F.; Waterman, C. M. Nanoscale architecture of integrin-based cell adhesions. *Nature* **2010**, *468* (7323), 580-584. DOI: 10.1038/nature09621

[55] Chen, W.; Shao, Y.; Li, X.; Zhao, G.; Fu, J. Nanotopographical surfaces for stem cell fate control: engineering mechanobiology from the bottom. *Nano Today* **2014**, *9* (6), 759-784. DOI: 10.1016/j.nantod.2014.12.002

[56] Curtis, A.S.G.; Forrester, J.V. The competitive effects of serum proteins on cell adhesion. *J. Cell Sci.* **1984**, *71*, 17-35.

[57] Schakenraad, J.M.; Busscher, H.J.; Wildevuur, C.R.H.; Arends, J. The influence of substratum surface free energy on growth and spreading of human fibroblasts in the presence and absence of serum proteins. *J. Biomed. Mater. Res.* **1986**, *20* (6), 773-784.

[58] Maiorano, G.; Sabella, S.; Sorce, B.; Brunetti, V.; Malvindi, M. A.; Cingolani, R.; Pompa, P. P. Effects of cell culture media on the dynamic formation of protein-nanoparticle complexes and influence on the cellular response. *ACS Nano* **2010**, *4* (12), 7481-7491. DOI: 10.1021/nn101557e

[59] Dessels, C.; Potgieter, M.; Pepper, M. S. Making the switch: alternatives to fetal bovine serum for adipose-derived stromal cell expansion. *Front. Cell Dev. Biol.* **2016**, *4*, 115. DOI: 10.3389/fcell.2016.00115

[60] Grinnell, F.; Feld, M.K. Fibronectin adsorption on hydrophilic and hydrophobic surfaces detected by antibody binding and analyzed during cell adhesion in serum-containing medium. *J. Biol. Cell.* **1982**, *257* (9), 4888-4893.

[61] Belot, N.; Rorive, S.; Doyen, I.; Lefranc, F.; Bruyneel, E.; Dedecker, R.; Micik, S.; Brotchi, J.; Decaestecker, C.; Salmon, I.; Kiss, R.; Camby, I. Molecular characterization of cell substratum attachments in human glial tumors relates to prognostic features. *Glia* **2001**, *36* (3), 375-390. DOI: 10.1002/glia.1124

[62] Andreu, I.; Luque, T.; Sancho, A.; Pelacho, B.; Iglesias-Garcia, O.; Melo, E.; Farre, R.; Prosper, F.; Elizalde, M. R.; Navajas, D. Heterogeneous micromechanical properties of the extracellular matrix in healthy and infarcted hearts. *Acta Biomater.* **2014**, *10* (7), 3235-3242. DOI: 10.1016/j.actbio.2014.03.034

[63] Ross, A. M.; Jiang, Z.; Bastmeyer, M.; Lahann, J. Physical aspects of cell culture substrates: topography, roughness, and elasticity. *Small* **2012**, *8* (3), 336-355. DOI: 10.1002/smll.201100934

[64] Jaggy, M.; Zhang, P.; Greiner, A. M.; Autenrieth, T. J.; Nedashkivska, V.; Efremov, A. N.; Blattner, C.; Bastmeyer, M.; Levkin, P. A. Hierarchical micro-nano surface topography promotes long-term maintenance of undifferentiated mouse embryonic stem cells. *Nano Lett.* **2015**, *15* (10), 7146-7154. DOI: 10.1021/acs.nanolett.5b03359

[65] Helenius, J.; Heisenberg, C. P.; Gaub, H. E.; Muller, D. J. Single-cell force spectroscopy. *J. Cell Sci.* **2008**, *121* (11), 1785-1791. DOI: 10.1242/jcs.030999

[66] Friedrichs, J.; Helenius, J.; Muller, D. J. Quantifying cellular adhesion to extracellular matrix components by single-cell force spectroscopy. *Nat. Protoc.* **2010**, *5* (7), 1353-1361. DOI: 10.1038/nprot.2010.89

[67] Friedrichs, J.; Legate, K. R.; Schubert, R.; Bharadwaj, M.; Werner, C.; Muller, D. J.; Benoit, M. A practical guide to quantify cell adhesion using single-cell force spectroscopy. *Methods* **2013**, *60* (2), 169-178. DOI: 10.1016/j.ymeth.2013.01.006

[68] Suresh, S. Biomechanics and biophysics of cancer cells. *Acta Biomater.* **2007**, *3* (4), 413-438. DOI:

10.1016/j.actbio.2007.04.002

[69] Turajlic, S.; Swanton, C. Metastasis as an evolutionary process. *Science* **2016**, *352* (6282), 169-175. DOI: 10.1126/science.aaf2784

[70] Guedes, A. F.; Carvalho, F. A.; Malho, I.; Lousada, N.; Sargento, L.; Santos, N.C. Atomic force microscopy as a tool to evaluate the risk of cardiovascular diseases in patients. *Nat. Nanotechnol.* **2016**, *11* (8), 687-692. DOI: 10.1038/nnano.2016.52

[71] Radmacher, M. Measuring the elastic properties of living cells by the atomic force microscope. *Methods Cell Biol.* **2002**, *68*, 67-90. DOI: 10.1016/S0091-679X(02)68005-7

[72] Gavara, N. A beginner's guide to atomic force microscopy probing for cell mechanics. *Microsc. Res. Tech.* **2017**, *80* (1), 75-84. DOI: 10.1002/jemt.22776

[73] Weaver, V.M. Cell and tissue mechanics: the new cell biology frontier. *Mol. Biol. Cell* **2017**, 28 (14), 1815-1818. DOI: 10.1091/mbc.E17-05-0320

[74] Diz-Munoz, A.; Weiner, O. D.; Fletcher, D. A. In pursuit of the mechanics that shape cell surfaces. *Nat. Phys.* **2018**, *14* (7), 648-652. DOI: 10.1038/s41567-018-0187-8

[75] Cross, S. E.; Jin, Y. S.; Rao, J.; Gimzewski, J. K. Nanomechanical analysis of cells from cancer patients. *Nat. Nanotechnol.* **2007**, *2* (12), 780-783. DOI: 10.1038/nnano.2007.388

[76] Plodinec, M.; Loparic, M.; Monnier, C. A.; Obermann, E. C.; Zanetti-Dallenbach, R.; Oertle, P.; Hyotyla, J. T.; Aebi, U.; Bentires-Alj, M.; Lim, R. Y. H.; Schoenenberger, C. A. The nanomechanical signature of breast cancer. *Nat. Nanotechnol.* **2012**, *7* (11), 757-765. DOI: 10.1038/nnano.2012.167

[77] Guilak, F.; Cohen, D. M.; Estes, B. T.; Gimble, J. M.; Liedtke, W.; Chen, C. S. Control of stem cell fate by physical interactions with the extracellular matrix. *Cell Stem Cell* **2009**, *5* (1), 17-26. DOI: 10.1016/j.stem.2009.06.016

[78] Murphy, W. L.; McDevitt, T. C.; Engler, A. J. Materials as stem cell regulators. *Nat. Mater.* **2014**, *13* (6), 547-557. DOI: 10.1038/nmat3937

[79] Mpoyi, E. N.; Cantini, M.; Reynolds, P. M.; Gadegaard, N.; Dalby, M. J.; Salmeron-Sanchez, M. Protein adsorption as a key mediator in the nanotopographical control of cell behavior. *ACS Nano* **2016**, *10* (7), 6638-6647. DOI: 10.1021/acsnano.6b01649

[80] Bettinger, C. J.; Langer, R.; Borenstein, J. T. Engineering substrate topography at the micro- and nanoscale to control cell function. *Angew. Chem. Int. Ed.* **2009**, *48* (30), 5406-5415. DOI: 10.1002/anie.200805179

[81] Calzado-Martin, A.; Encinar, M.; Tamayo, J.; Calleja, M.; San Paulo, A. Effect of actin organization on the stiffness of living breast cancer cells revealed by peak-force modulation atomic force microscopy. *ACS Nano* **2016**, *10* (3), 3365-3374. DOI: 10.1021/acsnano.5b07162

[82] Nematbakhsh, Y.; Pang, K. T.; Lim, C. T. Correlating the viscoelasticity of breast cancer cells with their malignancy. *Converg. Sci. Phys. Oncol.* **2017**, *3* (3), 034003. DOI: 10.1088/2057-1739/aa7ffb

[83] Wirtz, D.; Konstantopoulos, K.; Searson, P. C. The physics of cancer: the role of physical interactions and mechanical forces in metastasis. *Nat. Rev. Cancer* **2011**, *11* (7), 512-522. DOI: 10.1038/nrc3080

For Table of Contents Use Only

Nanotopographical surfaces for regulating cellular mechanical behaviors investigated by atomic force microscopy

Mi Li[1, 2*], Ning Xi[3], Yuechao Wang[1, 2], Lianqing Liu[1, 2*]

[1]State Key Laboratory of Robotics, Shenyang Institute of Automation, Chinese Academy of Sciences, Shenyang 110016, China

[2]Institutes for Robotics and Intelligent Manufacturing, Chinese Academy of Sciences, Shenyang 110016, China

[3]Department of Industrial and Manufacturing Systems Engineering, The University of Hong Kong, Hong Kong, China

*Corresponding authors (e-mail: limi@sia.cn; lqliu@sia.cn)